Crystal Structures of the Copper-Containing Amine Oxidase from *Arthrobacter globiformis* in the Holo and Apo Forms: Implications for the Biogenesis of Topaquinone[†,‡]

Matthew C. J. Wilce,[§] David M. Dooley,[||] Hans C. Freeman,*[,⊥] J. Mitchell Guss,*[,§] Hideyuki Matsunami,[#] William S. McIntire,[▽] Christy E. Ruggiero,[||] Katsuyuki Tanizawa,[#] and Hiroshi Yamaguchi[@,$]

School of Chemistry and Department of Biochemistry, University of Sydney, New South Wales 2006, Australia, Department of Chemistry and Biochemistry, Montana State University, Bozeman, Montana 59717-0340, Molecular Biology Division, Department of Veterans Affairs Medical Center, San Francisco, California 94121, Department of Biochemistry and Biophysics and Department of Anesthesia, University of California, San Francisco, California 94143, and Institute for Protein Research and Institute of Scientific and Industrial Research, Osaka University, Ibaraki, Osaka 567, Japan

Received July 23, 1997; Revised Manuscript Received October 15, 1997[⊗]

ABSTRACT: The crystal structures of the copper enzyme phenylethylamine oxidase from the Gram-positive bacterium *Arthrobacter globiformis* (AGAO) have been determined and refined for three forms of the enzyme: the holoenzyme in its active form (at 2.2 Å resolution), the holoenzyme in an inactive form (at 2.8 Å resolution), and the apoenzyme (at 2.2 Å resolution). The holoenzyme has a topaquinone (TPQ) cofactor formed from the apoenzyme by the post-translational modification of a tyrosine residue in the presence of Cu^{2+}. Significant differences between the three forms of AGAO are limited to the active site. The polypeptide fold is closely similar to those of the amine oxidases from *Escherichia coli* [Parsons, M. R., et al. (1995) *Structure* 3, 1171−1184] and pea seedlings [Kumar, V., et al. (1996) *Structure 4*, 943−955]. In the active form of holo-AGAO, the active-site Cu atom is coordinated by three His residues and two water molecules in an approximately square-pyramidal arrangement. In the inactive form, the Cu atom is coordinated by the same three His residues and by the phenolic oxygen of the TPQ, the geometry being quasi-trigonal-pyramidal. There is evidence of disorder in the crystals of both forms of holo-AGAO. As a result, only the position of the aromatic group of the TPQ cofactor, but not its orientation about the $C^{\beta}-C^{\gamma}$ bond, is determined unequivocally. In apo-AGAO, electron density consistent with an unmodified Tyr occurs at a position close to that of the TPQ in the inactive holo-AGAO. This observation has implications for the biogenesis of TPQ. Two features which have not been described previously in amine oxidase structures are a channel from the molecular surface to the active site and a solvent-filled cavity at the major interface between the two subunits of the dimer.

The structural characterization of copper-containing amine oxidases is of broad importance because these enzymes have a variety of essential functions in the metabolism of biogenic primary amines. Amine oxidases have been purified and characterized from numerous organisms, ranging from bacteria to plants and mammals. The enzymes catalyze the two-electron oxidative deamination of primary amines:

$$RCH_2NH_2 + O_2 + H_2O \rightarrow RCHO + NH_3 + H_2O_2 \quad (1)$$

Interest in copper-containing amine oxidases has grown recently for two reasons. First, the enzymes have emerged as members of a growing class of metalloproteins wherein an amino acid side chain is post-translationally modified in a self-processing reaction to form a redox-active cofactor. Among the amine oxidases considered here, an active-site tyrosine is oxidized to form 2,4,5-trihydroxyphenylalanine-quinone (TPQ).[1] In mammalian lysyl oxidases, an oxidized tyrosine is covalently cross-linked to the ϵ-amino group of a lysine residue, and has been designated "lysine tyrosylquinone" (LTQ). Second, evidence that an active-site radical, a semiquinone, may be a key catalytic intermediate is accumulating. Authoritative reviews on the biochemistry,

[†] This work was supported by Grants A29230677 and A29601726 from the Australian Research Council (to H.C.F. and J.M.G.), Grant GM27659 from the National Institutes of Health (to D.M.D.), a Merit Review grant from the U.S. Department of Veteran Affairs and Grant HL16251 from the National Institutes of Health (to W.S.M.), Grants-in-Aid 8214210 and 8249224 from the Ministry of Education, Science, Sports and Culture of Japan (to K.T.), and a grant from the Japan Society for the Promotion of Science (Research for the Future) (to K.T.). The use of synchrotron radiation facilities at the KEK Photon Factory, Tsukuba, Japan, was assisted by a travel grant from the Australian Access to Major Research Facilities Program.

[‡] Crystallographic coordinates for the active holo, inactive holo, and apo forms of *Arthrobacter globiformis* amine oxidase have been deposited with the Brookhaven Protein Data Bank as entries 1AV4, 1AV1, and 1AVK, respectively.

* To whom correspondence should be addressed. H.C.F.: phone, +61-2-9351-4405; fax, +61-2-9351-3329; e-mail, freemanh@chem.usyd.edu.au. J.M.G.: phone, +61-2-9351-4302; fax, +61-2-9351-4726; e-mail, M.Guss@biochem.usyd.edu.au.

[§] Department of Biochemistry, University of Sydney.

[||] Montana State University.

[⊥] School of Chemistry, University of Sydney.

[#] Institute of Scientific and Industrial Research, Osaka University.

[▽] Department of Veterans Affairs Medical Center and University of California.

[@] Institute for Protein Research, Osaka University.

[$] Current address: School of Science, Kwansei Gakuin University, Nishinomiya, Hyogo 662, Japan.

[⊗] Abstract published in *Advance ACS Abstracts,* December 1, 1997.

[1] Abbreviations: AGAO, *Arthrobacter globiformis* phenylethylamine oxidase; AO, amine oxidase; DPI, diffraction precision indicator; ECAO, *Escherichia coli* amine oxidase; esd, estimated standard deviation; M_r, relative molecular weight; PEG, polyethylene glycol; PSAO, pea seedling amine oxidase; rms, root mean square; TPQ, 2,4,5-trihydroxyphenylalaninequinone.

S0006-2960(97)01797-2 CCC: $14.00

mechanisms, and cofactor biogenesis of amine oxidases are available (*1*−*7*).

Crystal structures of two amine oxidases have been published: active, inactive and inhibitor-complexed forms of the enzyme from *Escherichia coli* (ECAO) (*8, 9*); and an active form of the pea seedling amine oxidase (PSAO) (*10*). The structure analysis of a second eukaryotic amine oxidase from the yeast *Hansenula polymorpha* is in progress (*11*). In the published structures, the polypeptide fold, the active-site structure, and the intersubunit contacts are clearly revealed. The ECAO and PSAO molecules are homodimers, comprising two subunits with four domains in the case of ECAO, and two subunits with three domains in PSAO. In the active form of both enzymes, the Cu(II) atom is coordinated by three histidine imidazole groups and two water molecules, the Cu(II) atom has a distorted square-pyramidal geometry, and the TPQ cofactor is close to the Cu(II) atom but not coordinated to it. The crystallographically determined Cu(II)-site dimensions are not yet known to high precision, but are consistent with the conclusions from numerous spectroscopic studies. The structure of ECAO was originally determined for an "inactive" form, in which the Cu(II) atom is coordinated by three histidine residues and by the TPQ cofactor. In this work, we have obtained evidence of both "active" and inactive forms of the phenylethylamine oxidase from *Arthrobacter globiformis* (AGAO).[2]

A central issue, for which structural information would be invaluable, concerns the mechanism of tyrosine oxidation to TPQ. This is a six-electron oxidation (eq 2). Kinetics and spectroscopic studies have shown that the unmodified (tyrosine-containing) apoprotein requires only copper and oxygen for stoichiometric TPQ formation (*12*−*14*). A preformed Cu(II) complex of AGAO has been shown to be competent with regard to TPQ formation upon the addition of O_2 (*14*).

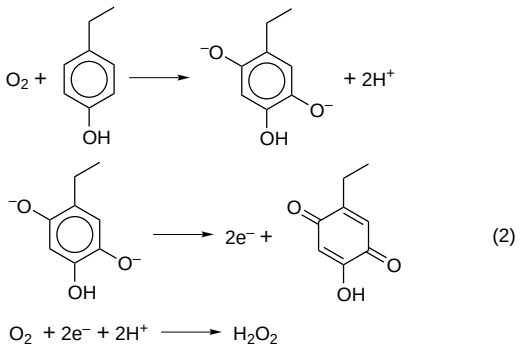

(2)

To date, the most extensive data on TPQ biogenesis have been obtained by studying *A. globiformis* phenylethylamine oxidase (AGAO). Here, we report the crystal structures of two forms of the resting state of the native enzyme [containing Cu(II) and TPQ], as well as the first structure of an apo amine oxidase, an inactive precursor form containing tyrosine.

MATERIALS AND METHODS

Enzyme Isolation and Purification. Wild-type AGAO was purified from *A. globiformis* (ATCC8010 = IFO12137) as described previously (*15*). Preparations used for crystallization displayed a single band upon SDS gel electrophoresis, and eluted as a single peak on HPLC (Mono-Q ion exchange).

Recombinant AGAO from *A. globiformis* was overproduced in *E. coli* as the Cu/TPQ-deficient apoprotein. Apo-AGAO was purified to homogeneity as described previously (*12*), as well as by a new method that avoids the use of ammonium sulfate and dithiothreitol (*14*). The protein was homogeneous as judged by SDS gel electrophoresis. The recombinant holo-AGAO and the wild-type holoenzyme purified from the organism showed essentially identical properties, e.g., copper content, steady-state kinetic parameters, subunit M_r by SDS−PAGE, and N-terminal sequence, except that the wild-type enzyme lacked Met1-Thr2 (*16, 17*). The presence of copper in the wild-type holoenzyme, and its absence from the recombinant apoenzyme, were demonstrated by inductively coupled plasma mass spectrometry (ICP-MS) and by atomic absorption spectrometry (AAS), using a Hewlett-Packard 4500 spectrometer and a Shimadzu AA-6400G flameless spectrometer, respectively.

Activity of AGAO under Crystallization Conditions. The catalytic competence of wild-type AGAO in solutions approximating those used for crystallization (see below) was tested by means of a coupled assay for H_2O_2 production with phenylethylamine as the substrate, and a spectrophotometric assay for benzaldehyde production from benzylamine (C. Hartmann and W. S. McIntire, unpublished work). The activity of AGAO in solutions containing Li_2SO_4 instead of $(NH_4)_2SO_4$ was also determined. The compositions of the solutions were as follows: (a) $(NH_4)_2SO_4$ (0.1 M−3.0 M) and KPO_4 buffer (0.1 M, pH 7.0) and (b) Li_2SO_4 (1.0 M) and KPO_4 buffer (8 mM, pH 7.0) with or without PEG-8000 (10% w/v). Under all these conditions, the enzyme retained not less than 20% of its activity in phosphate buffer (0.1 M, pH 7.0). The effects of Li_2SO_4 and $(NH_4)_2SO_4$ were closely similar, the reduction of the catalytic activity by both salts being consistent with the increased ionic strength of the solutions. For reasons which will be discussed later, the retention of even reduced catalytic activity in solutions containing $(NH_4)_2SO_4$ was unexpected. When the pH of a solution containing either Li_2SO_4 or $(NH_4)_2SO_4$ was raised from 7.0 to 8.1, there was a further decrease in activity, consistent with the pH profile of the enzyme (D. M. Dooley and K. Tanizawa, unpublished observations). The final activity in the presence of the high salt concentrations at pH 8.1 was close to the background level. Normal activity was restored by desalting and exchange into pH 7.0 buffer, showing that the effects of ionic strength and pH on the catalytic activity of AGAO are reversible.

Crystallization. Crystals were grown by the vapor-diffusion hanging-drop method. The precipitant was (i) for the crystals of holo-AGAO used to record data set I (see below), a mixture of $(NH_4)_2SO_4$ (1.0 M), PEG 8000 (10% w/v), and Tris buffer (0.1 M) at pH 8.7; (ii) for the crystals of holo-AGAO used to record data set II, a mixture of $(NH_4)_2$-

[2] The use of the terms active and inactive to describe two forms of the AO active site is based on the reactivity of ECAO crystals grown in the absence and presence of $(NH_4)_2SO_4$ (*8*). This work shows that the influence of $(NH_4)_2SO_4$ on the structure of AO crystals and the activity of AO solutions requires re-evaluation. As a matter of convenience when making comparisons, we here retain the terms active and inactive to denote the TPQ-OFF and TPQ-ON states of the AO active site.

Table 1: Statistics of Data Collection

protein	data set I (holo-AGAO, inactive)	data set II (holo-AGAO, active)	data set III (apo-AGAO)
X-ray source	rotating-anode, Rigaku RU-200	Photon Factory, beamline 6A2	rotating-anode, Rigaku RU-200
detector	image-plate, R-axis IIc	image plates, Sakabe camera	image-plate, R-axis IV
data collection mode	oscillation	Weissenberg	oscillation
temperature	ambient	ambient	ambient
wavelength (Å)	1.54	1.00	1.54
space group	*C*2	*C*2	*C*2
unit cell dimensions			
a, *b*, *c* (Å), β (deg)	158.2, 64.1, 92.9, 112.7	158.7, 64.6, 93.3, 113.5	158.7, 64.6, 93.3, 112.3
no. of crystals	3	1	1
no. of observations	33 361	105 840	58 200
no. of unique reflections	19 006	33 778	39 585
multiplicity	1.75	3.13	1.47
$d_{max}-d_{min}$ (Å)	50.0−2.8	8.0−2.2	50.0−2.2
overall completeness (%)	88.7	90.1	87.3
overall R_{merge} (%)	8.2	8.5	6.1

resolution range (Å)	completeness (%)	R_{merge}	resolution range (Å)	completeness (%)	R_{merge}	resolution range (Å)	completeness (%)	R_{merge}
50.0−6.0	80.6	5.0	8.0−4.5	80.0	3.7	50.0−15.0	72.1	3.3
6.0−4.8	88.4	6.3	4.5−3.6	86.2	4.4	15.0−10.0	76.8	2.0
4.8−4.2	88.8	6.7	3.6−3.2	89.5	5.0	10.0−7.5	79.8	2.4
4.2−3.8	89.5	7.6	3.2−3.0	91.3	6.9	7.5−5.0	83.2	3.6
3.8−3.5	90.7	8.4	3.0−2.7	93.1	9.5	5.0−3.5	86.6	5.4
3.5−3.3	90.6	9.8	2.7−2.6	93.6	13.1	3.5−3.0	87.7	9.0
3.3−3.15	90.1	12.5	2.6−2.5	93.4	17.4	3.0−2.8	88.2	12.8
3.15−3.0	90.3	14.0	2.5−2.4	92.0	21.5	2.8−2.5	88.3	16.5
3.0−2.9	89.9	17.7	2.4−2.3	90.6	28.2	2.5−2.3	87.9	19.4
2.9−2.8	88.8	21.0	2.3−2.2	90.0	31.3	2.3−2.2	87.7	20.8

SO_4 (1.3 M ≈ 25% saturated) and Tris buffer (0.1 M) at pH 8.1; and for the crystals of apo-AGAO used to record data set III, a mixture of potassium and sodium tartrate (0.2 M) and HEPES buffer (25 mM) at pH 6.8. The crystals of holo-AGAO were plates with dimensions of 0.2 mm × 0.4 mm × 0.1 mm, while the crystals of apo-AGAO were rods with dimensions of 0.8 mm × 0.2 mm × 0.2 mm. In each case, the diffraction symmetry and systematic absences were consistent with space group *C*2. The unit cell dimensions of all three forms (Table 1) were consistent with a solvent content of ∼58% and an asymmetric unit comprising one subunit of the homodimeric AGAO molecule.

The superlattice effects noted previously for crystals of holo-AGAO (*15*) varied greatly from crystal to crystal, and were found to disappear during the exposure of the crystals to X-rays at ambient temperature. The crystals used for data collection were specimens for which even the initial superlattice effects were weak. In view of the possibility of pH-dependent structural changes, it is important to note that the pH values cited above were those of the precipitant solution at the beginning of the crystallization experiments. The first crystals appeared after 5 months; data sets I and II were recorded after further intervals of 5 and 12 months (dictated by the growth of the crystals and the scheduling of synchrotron beam time). The effects of the efflux of time on the composition and pH of the mother liquor are uncertain. The precipitant solutions against which the crystals used for data sets I and II had been equilibrated still had pHs of ∼8.5 and ∼7.8, respectively, 18 months after the X-ray data were recorded.

Diffraction Data. The details and statistics of data collection are summarized in Table 1. The X-ray sources for data sets I and III were Rigaku RU-200 rotating-anode X-ray generators equipped with focusing mirror optics, the fine-focus filaments being 0.2 × 2.0 mm and 0.3 × 3.0 mm, respectively. Both data sets were recorded on R-axis image-plate detectors (model IIc for data set I and model IV for data set III). Data set II was recorded with synchrotron X-radiation (λ = 1.00 Å), using the Sakabe Weissenberg camera on beam line 6A2 at the KEK Photon Factory (Tsukuba, Japan). The data for holo-AGAO (data sets I and II) were processed, merged, and scaled using DENZO and SCALEPACK (*18*), and the intensities were converted to structure amplitudes using CCP4 programs (*19*). The data for apo-AGAO (data set III) were processed using PROCESS (*20*).

Structure Analysis and Refinements. At the beginning of the structure analysis, there was no reason to suspect that data sets I and II had been recorded from closely related but different forms of holo-AGAO. Under the circumstances, it appeared to be reasonable to merge the two sets of structure amplitudes, and this was done. The structure of holo-AGAO was initially solved using the merged data.

The phases for the structure analysis of holo-AGAO were found by molecular replacement. The search model was a truncated version of the ECAO molecule (Protein Data Bank entry 1OAC). The N-terminal domain D1 (which is not coded in the AGAO gene) and the copper atom were deleted, and all side chains were replaced by methyl groups. For the calculation of the rotation function, the 2-fold axis of the modified ECAO dimer was placed on the crystallographic *z*-axis, and the molecular center of mass was translated to the origin. The solution was found to be the fifteenth highest peak (α = 274.0°, β = 80.8°, and γ = 200.5°; sphere radius of 30 Å). The translation search was performed using one subunit of the modified ECAO dimer. The position giving the highest correlation coefficient was easily detected as the highest peak (fractional coordinates T_x = 0.1071, T_y = 0.0, and T_z = 0.4583).

The trial structure, comprising one subunit of the dimeric molecule, was refined in five stages. In the first stage, the entire subunit was subjected to rigid-body refinement. In the second stage, the three domains (D2−D4) were refined as separate but rigid bodies. At the end of this stage, the residuals were $R = 0.477$ and $R_{free} = 0.486$. In the third stage, the whole structure was refined by simulated annealing at 3000 K. The initial σ_A-weighted electron-density maps (*21*) could be easily interpreted in the region of domain D4, revealing numerous omitted side chains, but parts of domains D2 and D3 were not clearly defined. In the fourth stage, omit maps were calculated after deleting 10% of the structure at a time and subjecting the rest of the structure to simulated annealing at 1000 K. Appropriate harmonic restraints were applied to all atoms within 2 Å of the "omitted" portion of the structure, and bulk solvent corrections were included in all the calculations. Detailed examination of the omit maps led to extensive rebuilding of the structure and the identification of most of the missing side chains.

At this stage, the overall molecular structure had been determined unambiguously. The residual R and free residual R_{free} were 0.184 and 0.259, respectively. The active-site Cu atom with its three histidine and two water ligands was seen in the same relationship with the TPQ cofactor as in PSAO (*10*) so that the structure appeared to represent the active form of the enzyme. The electron density at the TPQ defined the position of the side chain, but was sufficiently noisy to leave the orientation of the aromatic quinone ring in doubt. The model included 258 solvent molecules. An unexpected feature of the model was that one of the Cu ligands, His592, appeared to be disordered.

In an attempt to trace the cause of the disorder at His592, we decided to examine the effect of refining the structure with each of the original data sets I and II separately. The separate refinements did not change the disorder at His592, but led to the surprising conclusion that data sets I and II had been recorded from crystals which contained holo-AGAO in two distinctly different states. The use of the merged data was therefore discontinued. The following account omits a large number of exploratory calculations, and summarizes the calculations which contributed to the final results.

The model obtained from the merged data was first modified by deleting the Cu atom, all active-site residues, and all solvent molecules. The model was then subjected to simulated annealing without reference to structure amplitudes. The aim was to produce a molecular model with minimal bias in the active-site region. This model was now refined with respect to data set I. The refinement was carried out by cycles of "simulated-annealing omit maps". A cycle comprised removing a segment of the model, submitting the rest of the model to simulated annealing at 1000 K, calculating electron-density difference maps, and refitting the model to these maps. In the final stage, the entire structure was again subjected to cycles of simulated annealing at 3000 K. The parameters treated as variables were the atomic coordinates and tightly restrained atomic temperature factors. The treatment of the atomic temperature factors was justified by the response of R_{free}. Although data set I covered the resolution range of 50−2.8 Å, the data in the range of 50−8 Å were relatively sparse and were not used in the refinement. Accordingly, no corrections for bulk solvent were included in the model refinement and map calculations. The result of the refinement was a model in which the structure of the Cu/TPQ site was closely similar to that of the inactive form of ECAO (*8*).[2] We shall refer to this model as inactive holo-AGAO. The refinement statistics are summarized in Table 2.

The close isomorphism between the three forms of AGAO led logically to the use of the inactive holo-AGAO structure as the starting model for the further calculations using data sets II and III. All atoms within 10 Å of the active-site Cu atom, the poorly defined loop at residues 46−50, and the solvent atoms were first deleted. New $\alpha_{calc(model)}$ phases were calculated from this model.

Using data set II (holo-AGAO), an electron-density difference map calculated with coefficients $[F_{obs(II)} - F_{obs(I)}]$ and with $\alpha_{calc(model)}$ phases immediately showed the positions of the active-site Cu, the three histidine ligands, and the TPQ cofactor. The configuration of the active site was similar to that obtained previously when using the merged data, consistent with the fact that the merged data were heavily dominated by data set II. Thus, it became apparent that data set II had been recorded from AGAO crystals in which the active site had a configuration analogous to that in PSAO (*10*). We shall refer to this model as active holo-AGAO.

Similarly, the refinement using data set III (apo-AGAO) commenced with an electron-density difference map calculated with coefficients $[F_{obs(III)} - F_{obs(I)}]$ and with $\alpha_{calc(model)}$ phases. Positive density in this map showed the position of the active-site Tyr382, while negative density confirmed the absence of the Cu atom. The subsequent refinement of the structures of active holo-AGAO and apo-AGAO followed the same protocol as that described for inactive holo-AGAO, the only differences being that all the data in the resolution range of 50−2.2 Å were used and that corrections for bulk solvent were included in the calculations. The refinement statistics for both structures are included in Table 2.

Software. The CCP4 program AMoRe (*22*) was used to compute the cross-rotation and the translation functions. The program used for the calculation of electron-density maps and simulated-annealing refinements with allowance for bulk-solvent corrections was X-PLOR, Version 3.8 (*23*). Model building was performed using O (*24*). Ramachandran plots were calculated using the program MOLEMAN and criteria described by Kleywegt and Jones (*25*).

The volumes of the internal cavities in the amine oxidase structures were calculated with program SURFNET (*26*), using a rolling sphere with a 1.4 Å radius. The illustrations of the cavities were prepared with program VOIDOO (*27*). The channels to the active site were visualized by generating a surface using GRASP (*28*) and were displayed in O (*24*).

RESULTS AND DISCUSSION

Three Types of AGAO Crystal. This work has revealed the structure of AGAO in two forms of the holoenzyme, and in the apoenzyme. While the two holo-AGAO structures exhibit effects that can reasonably be ascribed to mild disorder or heterogeneity, there is no doubt that they are different. This finding is unexpected. In both cases, the crystals which were used to record the X-ray data were grown in a NH_4^+-rich medium (see Crystallization). By analogy with ECAO (*8*), the exposure to NH_4^+ should have altered the enzyme structure by switching the active site to a

Table 2: Crystallographic Refinement Statistics and Stereochemical Parameters

protein	data set I (holo-AGAO, inactive)	data set II (holo-AGAO, active)	data set III (apo-AGAO)
$d_{max}-d_{min}$ (Å)	50.0−2.8	8.0−2.3	50.0−2.2
residues in the core ϕ,ψ region (%)	95.4	97.2	96.1
no. of non-hydrogen atoms	4959	5095	5042
no. of solvent atoms	122	258	205
average temperature factor			
main-chain atoms (Å^2)	27	20	36
side-chain atoms (Å^2)	29	22	37
solvent atoms (Å^2)	41	31	45
rms deviation from ideal values			
bond lengths (Å)	0.011	0.011	0.009
bond angles (deg)	1.8	1.7	1.6
refinement features	−	bulk solvent correction	bulk solvent correction
	−	anisotropic scaling	−
residual R (%)	15.0	20.0	19.4
free residual R_{free} (%)	20.2	24.1	23.7
fraction of data in the R_{free} set (%)	5	5	5
DPI[a] (Å)	−[b]	0.31	0.24

resolution range (Å)	residual R (%)	free residual R_{free} (%)	resolution range (Å)	residual R (%)	free residual R_{free} (%)	resolution range (Å)	residual R (%)	free residual R_{free} (%)
50.0−5.6	17.6	20.4	8.0−4.4	16.5	22.9	50.0−4.4	13.8	17.3
5.6−4.4	14.1	15.1	4.4−3.5	14.1	18.5	4.4−3.5	15.1	19.3
4.4−3.9	13.9	19.2	3.5−3.1	16.5	19.8	3.5−3.1	19.9	23.4
3.9−3.5	14.2	19.6	3.1−2.8	19.9	24.2	3.1−2.8	24.6	27.1
3.5−3.3	15.1	21.8	2.8−2.6	21.9	27.7	2.8−2.6	27.4	33.2
3.3−3.1	16.4	25.9	2.6−2.4	23.6	27.8	2.6−2.4	28.8	35.3
3.1−2.9	17.3	34.5	2.4−2.3	25.3	26.8	2.4−2.3	28.8	34.9
2.9−2.8	16.9	31.0	2.3−2.2	26.6	29.9	2.3−2.2	30.2	36.3

[a] DPI = diffraction precision indicator = $1.0(N/P)^{1/2}C^{-1/3}d_{min}R$, where N = number of atoms, P = number of degrees of freedom = number of independent reflections − number of variables, C = completeness of data, d_{min} = resolution, and R = residual (*41*). [b] No DPI is shown for data set I, where the number of degrees of freedom as defined above is negative. The DPI does not take into account the additional "observations" represented by restraints (*41*).

configuration in which the Cu atom is four-coordinate and the TPQ cofactor is one of the ligands. We find that this occurred only in the crystals which were used to record data set I, where the configuration of the active site is indeed analogous to the inactive form of ECAO (*8*). In the structure derived from data set II, the configuration of the active site is analogous to the active form of PSAO (*10*). In further contrast with the reported behavior of the enzyme in ECAO crystals, AGAO solutions remain catalytically active even in the presence of a high concentration of $(NH_4)_2SO_4$ (see Activity of AGAO). It has thus become clear that the transitions and equilibria between the inactive and active forms of AOs require further study. Subject to this caveat, we shall continue using the descriptions inactive and active interchangeably with TPQ-ON and TPQ-OFF in this work, since this will facilitate some comparisons.[2]

The final model of all three structures comprises residues 9−628 and a number of solvent molecules (see Table 2). A loop at residues 46−50 is included but consistently lies in weak electron density. Residues 1−8 and 629−638 do not lie in density, and are excluded. (In wild-type holo-AGAO, residues 1 and 2 are in any case absent from the sequence.) The models for inactive holo-AGAO, active holo-AGAO, and apo-AGAO have average disorder parameters (temperature factors) ⟨B⟩ of 28, 20, and 37 Å^2, respectively, and the proportions of their residues other than glycines lying within the core region of a Ramachandran plot (not shown) are 97%, 95, and 96, respectively. These and other refinement statistics are shown in Table 2.

Validity of Comparisons between the Three AGAO Structures. Since the models for the three forms of AGAO are based on data sets which differ in resolution and degree of completeness (Table 1), we emphasize that the models were refined separately and that the calculations included the extensive use of simulated-annealing omit maps. The existence of real differences between the active-site regions of the two fully refined holo-AGAO models was further confirmed by "crossover omit maps"; each model minus its active site was subjected to a further cycle of simulated-annealing refinement against the data set of the other model. In each case, an $F_{obs} - F_{calc}$ omit map calculated after the refinement confirmed the position of the TPQ side chain which had been deduced previously from that data set.

Comparisons between the apo- and holo-AGAO models are unlikely to be prejudiced by the fact that the apo-AGAO crystals were prepared from recombinant protein, whereas the protein used for the crystallisation of holo-AGAO was derived from the wild-type organism. As already mentioned, the recombinant apo-AGAO can be converted to holo-AGAO with the same (i) N-terminal sequence, (ii) subunit M_r (by SDS−PAGE), (iii) copper content, and (iv) steady-state kinetic parameters for phenylethylamine oxidation as holo-AGAO from the wild-type organism (see Enzyme Isolation and Purification).

Polypeptide Folds of Holo- and Apo-AGAO. The polypeptide folds of apo-AGAO and both forms of holo-AGAO are identical within the limits of precision. The same N- and C-terminal residues lie in weak or nonexistent electron density. When the active and inactive forms of holo-AGAO are superimposed, the rms difference between the main chain atomic positions is 0.2 Å; the corresponding rms difference between apo- and active holo-AGAO is 0.4 Å. On the other hand, the average disorder parameter (temperature factor) ⟨B⟩ in apo-AGAO (37 Å^2) is significantly larger than that in

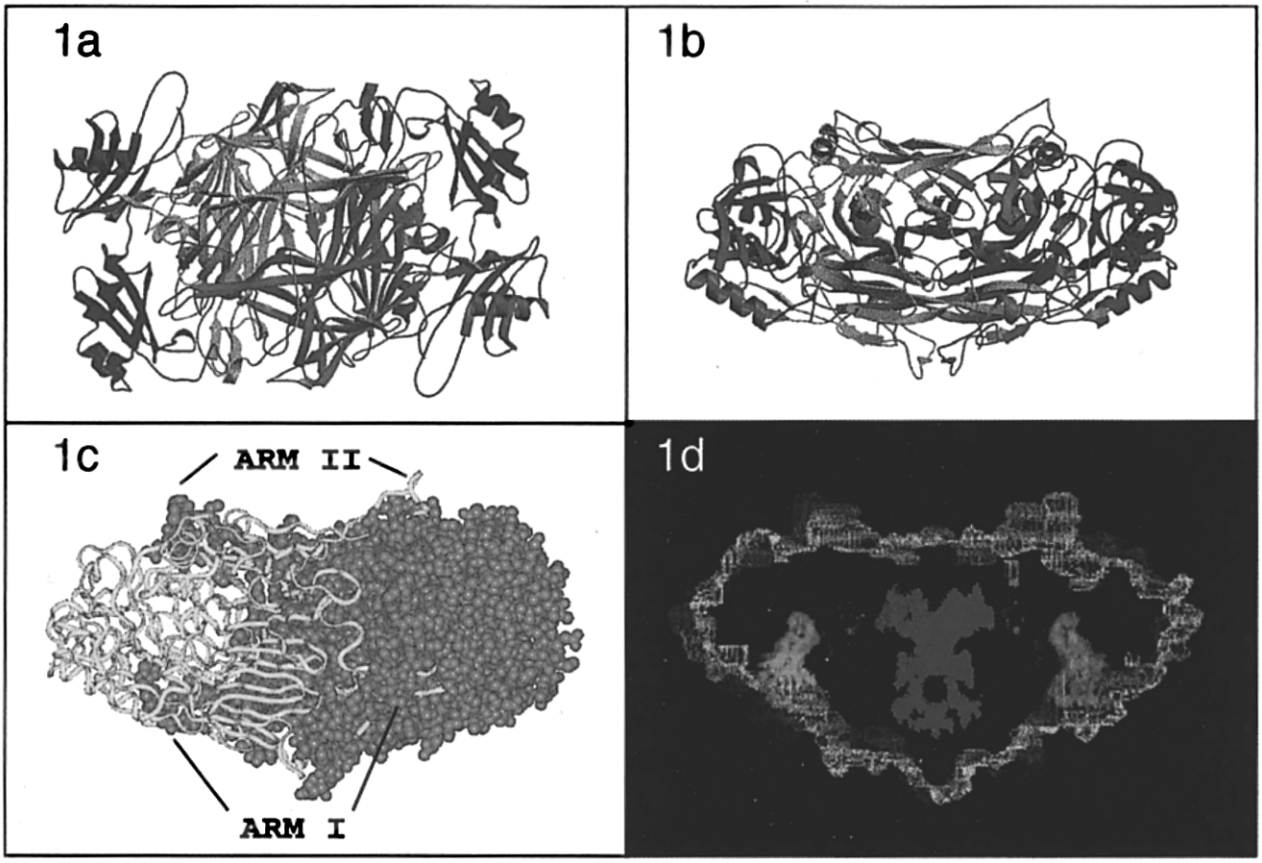

FIGURE 1: Four views of the *A. globiformis* amine oxidase molecule. (a) Ribbon diagram of the dimer viewed along its 2-fold symmetry axis: domain 2, red; domain 3, green; and domain 4, magenta and yellow. The Cu atom at the active site of each subunit is shown as a blue sphere. This Figure was drawn with MOLSCRIPT (*42*) and RASTER3D (*43*). (b) The AGAO dimer viewed along a direction perpendicular to the 2-fold symmetry axis. Colors as in panel a. (c) The AGAO dimer in an orientation similar to that in panel b. One subunit is represented as a yellow ribbon and the other as a red space-filling model. The two arms that originate from each subunit and grasp the other subunit are seen clearly. Much of arm II (the upper arm in this orientation) is exposed, whereas arm I fits into a groove on the surface of the other subunit and is only partly visible. This figure was generated using INSIGHT II (Biosym/MSI, San Diego, CA). (d) A section through the AGAO dimer, showing the molecular boundary (yellow), the solvent-filled cavity (green), and the channels to the two active sites (red). The Cu atom, the side chains of the three Cu-binding histidine residues, and the TPQ cofactor at each of the two active sites are also shown. The TPQ lies on the side of the active site remote from the solvent-filled cavity. The molecular boundary is a 1.4 Å rolling-sphere surface. The cavity is represented by a van der Waals surface. [Both surfaces were calculated using VOIDOO (*27*) and were drawn using O (*24*).]

holo-AGAO (inactive, 28 Å^2; active, 20 Å^2). It is possible that the larger $\langle B \rangle$ indicates a less rigid structure, which would be consistent with the observation that apo-AGAO is more susceptible to proteolysis than holo-AGAO (R. Matsuzaki and K. Tanizawa, unpublished work).

The molecular structure of AGAO is shown in panels a and b of Figure 1. The molecule is a homodimer with an M_r of 70 737 per subunit (calculated from the sequence including Met1-Thr2, Cu and TPQ). As in PSAO, the shape resembles a mushroom cap with dimensions of 110 × 65 × 45 Å. Each subunit of the dimer is composed of three domains, labeled D2−D4, which closely resemble the three C-terminal domains in PSAO and ECAO (the comparison necessarily excludes the 8 N-terminal and 10 C-terminal residues in AGAO, since these were not included in the model; see Materials and Methods). In AGAO, the large 18-stranded β-sandwich domain D4 is composed of residues 229−623. Domains D2 (residues 9−91) and D3 (residues 103−203) are located on the surface of D4. The α/β-roll topology found in PSAO and ECAO is conserved, but the positions of both domains in relation to D4 are slightly different.

Two conspicuous β-ribbon arms extend from each D4 domain to embrace the D4 domain of the other subunit. In the orientation of Figure 1b, Arm I (residues 348−369) lies in a groove along the bottom of D4; Arm II (residues 453−474) lies primarily along the surface at the top of the D4 domain (Figure 1c). The functional importance of these two arms is still uncertain. We shall suggest below that they not only contribute to the stability of the dimer but also affect the access of substrates to the active site. The active site of each subunit is located within domain D4, between the two arms from the other subunit, and close to the D4−D4 interface (Figure 1a,b).

Active Site in the Two Forms of Holo-AGAO. The only significant differences between the three forms of AGAO occur at the active site (Figure 2). While the differences are unequivocal, the limited precision of the active-site dimensions (Table 3) permits only qualitative descriptions and comparisons.

In active holo-AGAO (Figure 2a), the Cu(II) atom is coordinated by the imidazole groups of three histidine residues and by two water molecules, resulting in an approximately square-pyramidal geometry. The three histidines and one water, O_{eq}, are the "equatorial" ligands. The other water, O_{ax}, is the "axial" ligand. At His431 and His433, the Cu atom is bonded to $N^{\epsilon 2}$, while at His592, it is bonded to $N^{\delta 1}$. The orientation of each imidazole ring is

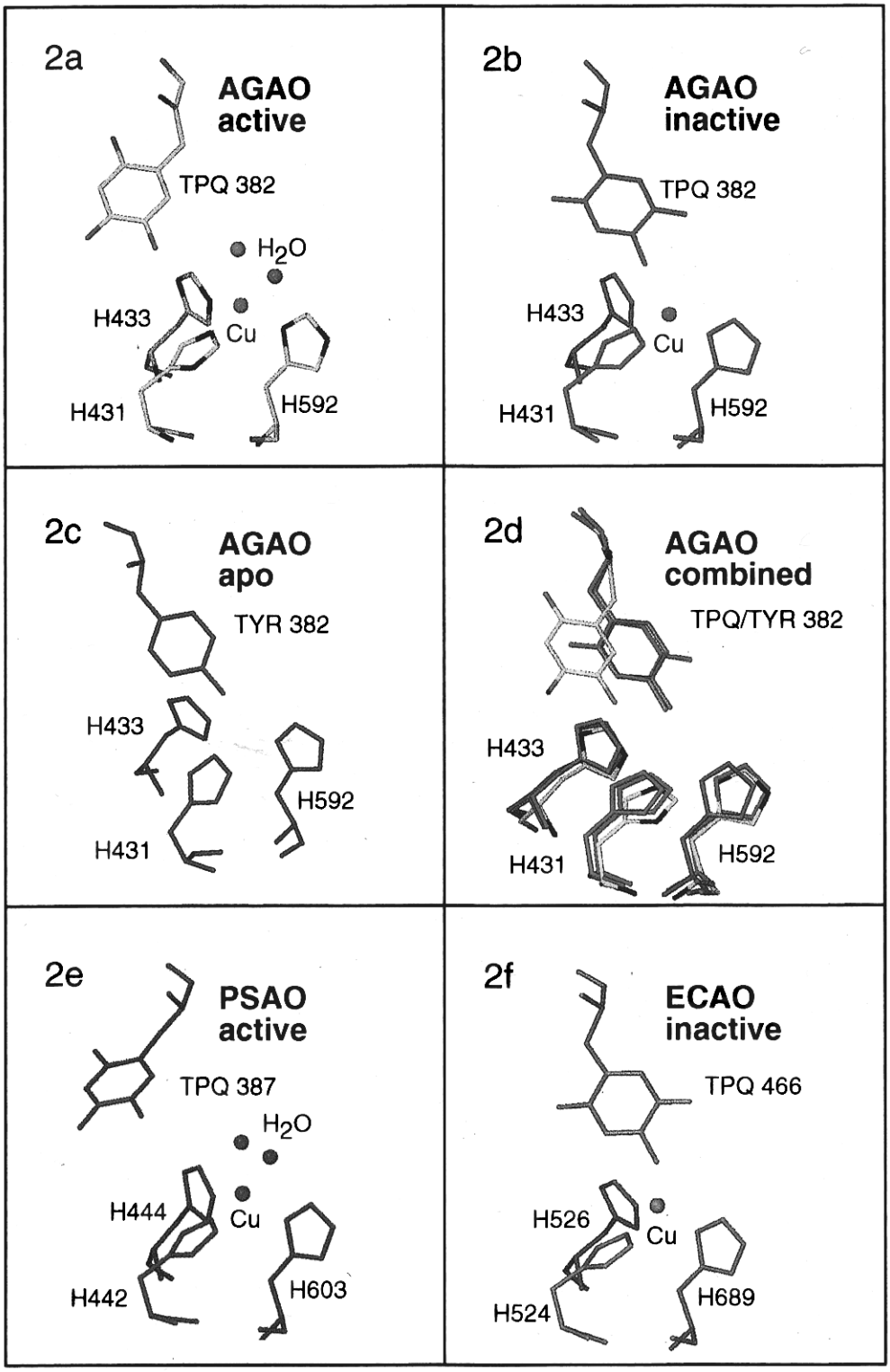

FIGURE 2: Active site in (a) the active form of holo-AGAO, (b) the inactive form of holo-AGAO (cyan), (c) apo-AGAO (red), (d) a superposition of the three forms of AGAO, (e) the active form of PSAO (green), and (f) the inactive form of ECAO (violet-red). The Cu atom and the two coordinated H_2O molecules are shown as blue and red spheres, respectively.

stabilized by a hydrogen bond from the free imidazole N atom (His431 $N^{\delta 1}\cdots$O Pro429, His433 $N^{\delta 1}\cdots$HO Tyr384, and His592 $N^{\epsilon 2}\cdots O^{\delta 1}$ Asp598) (Figure 4a). The water ligands O_{ax} and O_{eq} are hydrogen bonded outside the coordination sphere to an uncoordinated water molecule ($O_{ax}\cdots O_w$-$172\cdots O_{eq}$).

The position of the TPQ cofactor, residue 382, is defined by the electron density, but two orientations of the quinone group differing by a rotation of ~180° about the $C^{\beta}-C^{\gamma}$ bond are equally probable at the present resolution. The electron density is consistent with both orientations of C=O2, but there is no density at all for C=O5 (Figure 3a). Since the electron density may merely be reflecting the limited resolution and completeness of the diffraction data, it would be premature to conclude that the TPQ ring is disordered or rotating. When the TPQ side chain is in the same orientation as in the active form of PSAO, its closest contact with the Cu atom occurs at O5 (4.6 Å). However, there is an indirect

Table 3

(a) Dimensions of the Cu Site in AGAO[a]

bond/angle	TPQ-OFF	TPQ-ON
Cu−$N^{\epsilon 2}$ (His431)	2.1	2.0
Cu−$N^{\epsilon 2}$ (His433)	2.1	2.1
Cu−$N^{\delta 1}$ (His592a)	2.2	2.2
Cu−$N^{\delta 1}$ (His592b)	2.7	3.0
Cu−$O_{w(eq)}$	2.2	−
Cu−$O_{w(ax)}$	2.7	−
Cu−O4 (TPQ382)	−	2.4
N (His431)−Cu−N (His433)	99	91
−$N^{\delta 1}$ (His592a)	91	89
−$N^{\delta 1}$ (His592b)	128	120
−$O_{w(eq)}$	168	−
−$O_{w(ax)}$	94	−
−O4 (TPQ382)	−	75
N (His433)−Cu−N (His592a)	154	146
−N (His592b)	87	92
−$O_{w(eq)}$	88	−
−$O_{w(ax)}$	100	−
−O4 (TPQ382)	−	102
N (His592a)−Cu−N (His592b)	69	59
−$O_{w(eq)}$	88	−
−$O_{w(ax)}$	104	−
−O4 (TPQ382)	−	111
N (His592b)−Cu−$O_{w(eq)}$	64	−
−$O_{w(ax)}$	137	−
−O4 (TPQ382)	−	160
$O_{w(eq)}$−Cu−$O_{w(ax)}$	74	−

(b) Dihedral Angles at Two Active-Site Residues in AGAO

		TPQ382/Tyr382			His592 normal conformer a			His 592 alternate conformer b		
dihedral angle[c]	symbol	TPQ-OFF[b]	TPQ-ON[b]	apo[b]	TPQ-OFF	TPQ-ON	apo	TPQ-OFF	TPQ-ON	apo
C−N−C^{α}−C	ϕ	−93	91	97	101	−110	−113	103	−113	−113
N−C^{α}−C−N	ψ	137	143	148	104	112	112	107	118	112
N−C^{α}−C^{β}−C^{γ}	χ_1	40	−86	−76	−169	−173	−176	−88	−93	−91
C^{α}−C^{β}−C^{γ}−C^{δ}/N^{δ}	χ_2	−122	−50	−62	−177	−162	−176	178	154	−178

[a] $O_{w(eq)}$, $O_{w(ax)}$, His592a, and His592b denote the equatorial O (water) ligand, the axial O (water) ligand, and the normal and alternate conformers of His592, respectively. O4 (TPQ382) is the phenolic O atom of the TPQ cofactor. The first section of part a shows bond lengths (angstroms). The second section of part a shows bond angles (degrees). The Cu−ligand bond lengths and ligand−Cu−ligand bond angles are subject to probable errors of ∼0.2 Å and ∼5°, respectively. [b] TPQ-OFF, TPQ-ON, and apo represent active holo-AGAO, inactive holo-AGAO, and apo-AGAO, respectively. [c] The values of the dihedral angles are subject to probable errors of 5−10°.

link between the TPQ and the Cu atom via an uncoordinated water molecule and the axial water ligand (TPQ382 O5···O_w-76···O_{ax}−Cu) (Figure 4a). In the alternative orientation of the TPQ side chain, the closest contact with the Cu atom occurs at O2 (4.5 Å). In both orientations, the only residue which is unequivocally hydrogen bonded to the TPQ aromatic ring is the invariant Tyr284 (Figure 4b). There are in fact two 2.3 Å contacts between TPQ382 and Tyr284 (TPQ O4···HO Tyr284, TPQ O5···HO Tyr284). Comparisons with PSAO and ECAO suggest that the ambiguity may be real, i.e., that the hydrogen bond is bifurcated. Tyr284 in AGAO corresponds to Tyr286 in PSAO and Tyr369 in ECAO. In PSAO, Tyr286 is hydrogen bonded to TPQ O5 (*10*). In the ECAO−inhibitor complex, Tyr369 is hydrogen bonded to TPQ O4 (*9*). It is noteworthy that the latter contact, like that in AGAO, is exceptionally short (2.3 Å), implying that a proton is shared after ionization at TPQ O4 (*9*). Ionization of the phenolic group was also suggested by the formation of a hydrogen bond between TPQ O4 and the variable residue Lys296 in PSAO (*10*). The hydrogen bonds and salt linkages in the vicinity of the AGAO active site are listed in Table 4.

In the current model, the closest contact between the TPQ cofactor and the putative active-site base Asp298 is 3.6 Å, and the bond angles at the donor and acceptor atoms are outside the normally accepted range of values for a hydrogen bond (Table 4). The absence of a hydrogen bond between the TPQ side chain and Asp298 would be consistent with the relatively high pH (pH ∼8), at which the crystals of active holo-AGAO were grown. It has been shown that, in the resting state of bovine serum AO, the active-site base that abstracts an α-proton from amine substrates has a pK_a of about 8.0, which is unusually high for a carboxyl group (*29*). If it is assumed that Asp298 is the active-site base in AGAO and that its pK_a is similar to that in bovine serum AO, then at pH ∼8, its carboxyl must be at least partly in the charged form (COO^-) and therefore unfavorable for hydrogen bonding to TPQ C═O2. One result of this would be reduction of the restraints on the orientation of the TPQ ring. In contrast, in crystals of PSAO prepared at pH 4.8, the putative active-site base Asp300 is substantially protonated and able to stabilize the orientation of the TPQ ring by forming a 2.7 Å hydrogen bond to TPQ C═O2 (*10*).

Several hydrogen bonds and salt linkages in the immediate vicinity of the TPQ (Figure 4b) appear to be part of a network involving a conserved residue, His355, and a conservatively substituted residue, Lys354, on Arm I. The side chain of His355 interacts with the carboxylate group of the conserved residue Asp383, adjacent to the active-site TPQ382. The

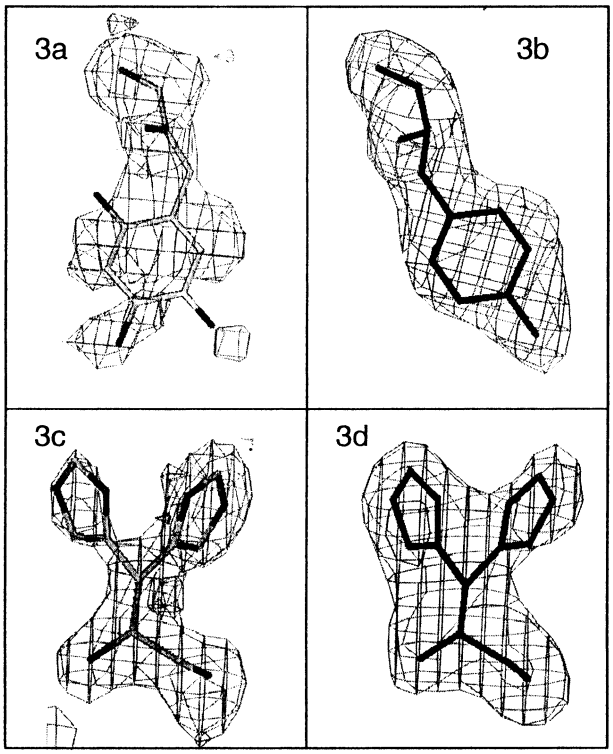

FIGURE 3: Electron density ($F_{obs} - F_{calc}$) omit maps for (a) TPQ382 in holo-AGAO, (b) Tyr382 in apo-AGAO, (c) His592 in holo-AGAO, and (d) His592 in apo-AGAO. The contours are drawn at the 1$\sigma(\rho)$ level. Panels a and b illustrate the quality of the current 2.2 Å electron density maps in the vicinity of the active site. Panels c and d show the two conformers of His592 and the difference between their relative contributions to the holo- and apo-AGAO structures.

side chain of Asp383 in turn forms a hydrogen bond to the side chain of another conserved residue, Thr378. The side chain of Lys354 interacts with the carboxylate group of Asp316, creating an additional link from arm I to a different part of the domain D4 polypeptide. Analogous interactions occur in the other crystallographically characterized AO structures (see below).

Disorder at a Cu-Binding Histidine. A puzzling feature of the current model for the active site in active holo-AGAO is the fact that the side chain of His592 appears to have a second conformer (Figure 3c). The second conformer is effectively the same as in apo-AGAO (see below), and is estimated to represent at most 20% of the structure. When His592 is in the normal conformation ("a"), the coordination geometry of the Cu atom is approximately square-planar, in agreement with the Cu sites in PSAO and ECAO. When His592 is in the alternative conformation ("b"), the Cu−$N^{\delta 1}$ (His592) bond length is ∼2.7 Å, and the bond angles at the Cu atom are unlike those for any acceptable coordination geometry (Table 3a). While electron-density maps leave no doubt that conformer b is present in the crystals, there is a strong possibility that it occurs only in molecules which have lost their Cu atom. In Cu-free AGAO molecules, His592 may well adopt a conformation different from a, since the void left by the removal of the Cu atom must be filled. The fact that conformer b is similar to one of the conformers in apo-AGAO is consistent with this hypothesis, which is equivalent to saying that the crystals of holo-AGAO include a proportion of Cu-free molecules. Further, the presence of two significantly different coordination geometries should be spectroscopically distinguishable, but Cu(II) EPR spectra of frozen solutions of the wild-type enzyme have so far not provided any evidence of two types of copper. We intend to pursue this question in future work. For the time being, we note that loss of copper may have occurred chemically during the long period when the crystals were in contact with the crystallization medium, or physically as a result of radiation damage during the X-ray exposures.

In the inactive form of holo-AGAO, the Cu(II) is coordinated by the same three His residues as in the active form, plus the TPQ (Figure 2b). Phenolic oxygen atom O4 of TPQ382 lies in approximately the position which the axial water ligand occupies in the active holoprotein, i.e., about 2.8 Å from the Cu atom. His592 exists as the same two conformers, with approximately the same Cu−$N^{\delta 1}$ distances and occupancies as in active holo-AGAO. The 2.8 Å resolution electron-density maps do not resolve coordinated or uncoordinated solvent in the active-site region, and the coordination geometry of the Cu atom is not well-defined. The bond directions correspond to distorted trigonal-pyramidal coordination with $N^{\epsilon 2}$ (His431) at the apex of the pyramid; however, small movements of the other two histidines would suffice to make the coordination tetrahedral, while the addition of a water molecule could make it square-pyramidal or trigonal-bipyramidal.

Precursor Active Site in Apo-AGAO. Apo-AGAO has no Cu atom, and Tyr382 is present in its unmodified state (Figures 2c and 3b). The absence of Cu was confirmed both by electron-density maps and by ICP-MS and AAS (see Materials and Methods). Two of the three histidine side chains which are to become the Cu ligands, His431 and His433, are in approximately the same positions and orientations as in the holoenzyme. The third histidine, His592, again has two conformers (a and b), their relative occupancies being estimated as ∼40 and ∼60%, respectively (Figure 3d). Both conformers of His592 have their side chain displaced by about 0.7 Å in the direction of the future Cu position, thus accounting for part of the space which the Cu atom is to occupy (Figure 2d). The position of the Tyr382 side chain is close to that of the TPQ382 side chain in the inactive form of holo-AGAO, and is stabilized by a hydrogen bond from the phenolic hydroxyl group to the imidazole ring of His431 (Tyr382 O4···$N^{\delta 1}$ His431). Only a single water molecule, equivalent to O_w76 in the active form of holo-AGAO, has been located, and is within hydrogen-bonding distance of the phenolic hydroxyl group of Tyr382. Apart from these differences involving Tyr382, the hydrogen bonds in the active-site region are, within the limits of precision, the same as in the active holo-AGAO structure. All these features have been confirmed by electron-density difference and omit maps.

A Solvent-Filled Cavity. The structure analysis of AGAO has revealed a large water-filled cavity between the D4 domains of the two subunits (Figure 1d). The volume of the cavity is ∼3950 $Å^3$, corresponding to ∼130 water molecules. One section of the wall of the cavity is formed by a segment of β-sheet which includes two of the Cu-binding histidine residues at the active site, His431 and His433. The backbone atoms of these histidine residues are in contact with the solvent in the cavity. There is no connection between the cavity and the external solvent, but relatively small changes in the polypeptide structure would permit such a connection to be made. Despite the possibility of such rearrangements, the cavity is unlikely to be a pathway

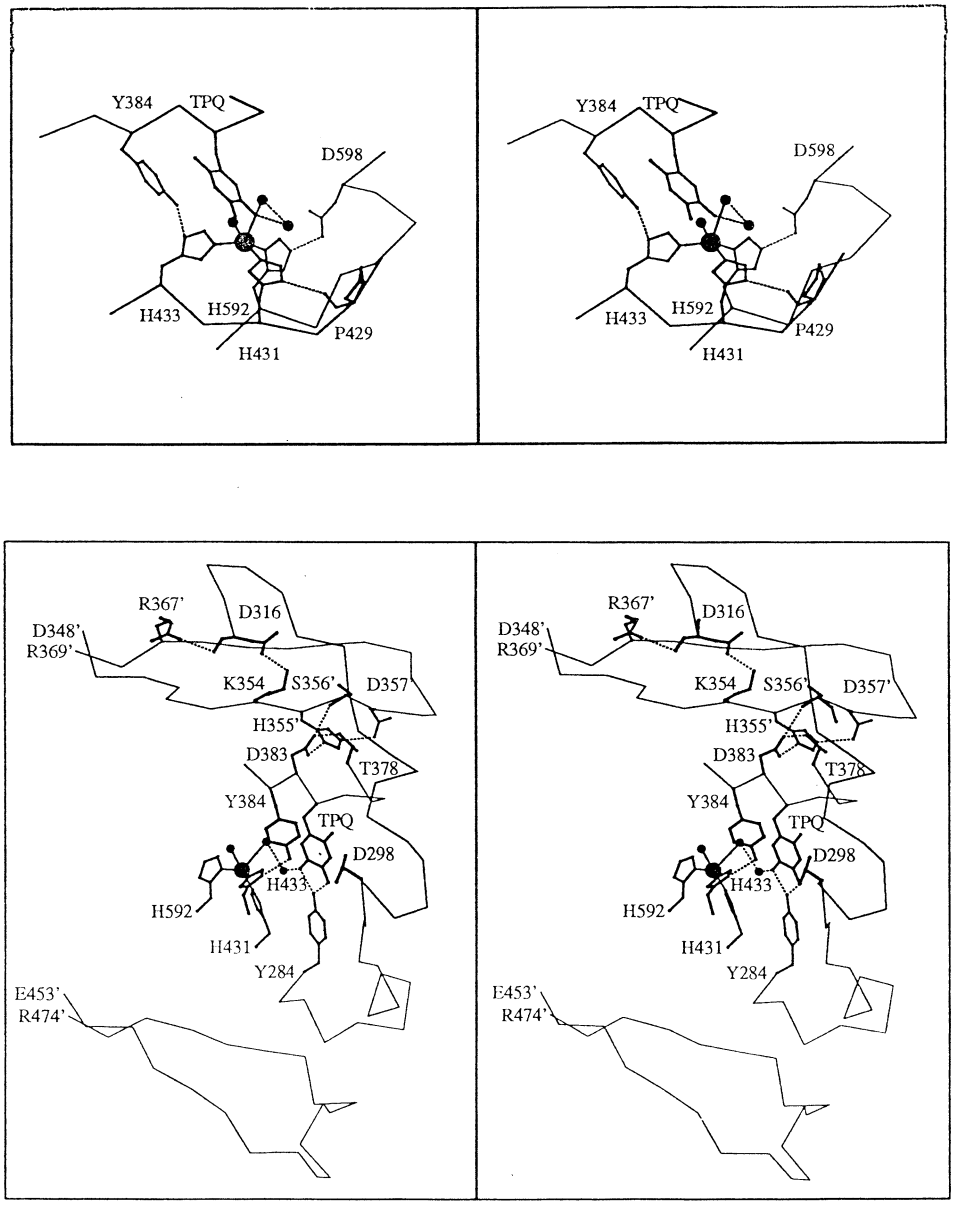

FIGURE 4: Stereodiagrams showing hydrogen-bonded interactions in the immediate vicinity of the active site in holo-AGAO. (Top) Hydrogen bonds at the three Cu-binding histidine residues (His431, His433, and His592) and at the TPQ cofactor. (Bottom) Hydrogen bonds involving other active-site residues. The upper arm corresponds to arm I in Figures 1c and 8. Residues Tyr284, Asp298, Asp316, Thr378, Asn381, His355, His431, His433, and His592 are conserved in all known amine oxidase sequences, while Lys354 and Asp383 are conservatively substituted. Comparable data for PSAO have been reported (*10*).

between the solvent and the active site for substrate amines and product aldehydes (see below).

A Channel to the Active Site. This work has also revealed a hitherto unreported channel, which seems to be suitable for the movement of reactants and reaction products to and from the active site (Figure 5). The channel originates in a region of the molecular surface near the junction of domains D3 and D4 . The molecular surface surrounding the entrance to the channel is predominantly negative (Figure 5a), the charges being associated with the side chains of Glu102, Glu103, Glu106, and Glu109 of domain D3 and Asp357′ on arm I from domain D4 of the other subunit of the dimer. The internal surface of the channel is lined by residues which become more hydrophobic as the active site is approached (Figure 6). A residue near the end of the channel, Tyr296, can be modeled in several orientations, and appears to be a "gate" to the active site. In one orientation, the side chain of Tyr296 blocks access to the active site; in other orientations, it permits unhindered access. In apo-AGAO (where only Cu^{2+} ions and O_2 molecules need access to the active site), the gate is closed. In the electron-density maps for both forms of holo-AGAO, the density for the side chain of Tyr296 is missing, consistent with disorder.

Titratable Cysteine Residues. AGAO has four Cys residues (Cys315, Cys317, Cys343, and Cys636). Two of the thiol groups can be titrated with 5,5′-dithiobis(2-nitrobenzoic acid) in the apoprotein, whereas none is titratable in the holoprotein (Matsuzaki, R., & Tanizawa, K., unpublished work). The reason is not obvious. The three AGAO structures provide clear evidence of only one intramolecular disulfide bridge, (Cys317)S−S(Cys343), which is found also in PSAO but not in ECAO. Thus, the question of whether Cys315 and Cys636 form disulfide bridges to a Cys in another molecule or subunit arises. This is unlikely. In the case of Cys315, the side chain is seen in electron-density maps and lies near the surface of domain D4, but its

Table 4: Hydrogen Bonds and Salt Bridges in the Vicinity of the Active Site in Active Holo-AGAO[a,b]

atoms	distance (Å)
(a) Interactions Involving a Cu-Binding His Residue	
His431 $N^{\delta1}$···O *Pro429*	3.0
His433 $N^{\delta1}$···O^{η} *Tyr384*	2.7
His592 $N^{\epsilon2}$···$O^{\delta1}$ Asp598	3.0
(b) Interactions Involving the TPQ Cofactor[c]	
TPQ382 O2···O Ile379	2.8[d]
TPQ382 O2···$O^{\delta1}$ Asp298	3.6[e]
TPQ382 O4···O^{η} Tyr284	2.3
TPQ382 O5···O^{η} Tyr284	2.3
TPQ382 O5···O_w76···O_w77-Cu	2.9, 3.1
TPQ382(alt) O5···$N^{\delta2}$ Asn381	3.6[e]
(c) Interactions Involving Other Side Chains in Domain D4	
Gln294 $O^{\epsilon1}$···O^{η} *Tyr296*	3.2
Gln294 $N^{\epsilon2}$···$O^{\delta1}$ *Asn295*	2.7
Asp316 $O^{\delta2}$···N Glu312	2.8
Thr378 O^{γ}···$O^{\delta1}$ Asp383	2.7
Asn381 $N^{\delta2}$···O Val405	2.7
(d) Interactions Involving Residues on Arm I of the Second Subunit[c]	
Lys354′ N^{ζ}···$O^{\delta1}$ Asp316	2.6
Lys354′ N···O^{γ} Thr403	3.1
Lys354′ O···N Gly404	3.1
His355′ $N^{\epsilon2}$···$O^{\delta2}$ Asp357′	3.1
His355′ $N^{\delta1}$···$O^{\delta2}$ Asp383	2.6
Ser356′ N···$O^{\delta1}$ Asp316	3.2
Arg367′ N^{η}···O Asp383	3.0
(e) Interactions Involving Residues on Arm II of the Second Subunit[c]	
Asn468′ $O^{\delta1}$···O Tyr284	3.0
Phe470′ O···$N^{\delta2}$ *Asn418*	3.1
(f) Peptide−Peptide Interactions Involving Residues Listed in Parts a−e	
Val282 N···O *Tyr296*	2.7
Tyr284 N···O Gly294	3.2
Gln294 N···O Arg291	2.8
Tyr296 N···O Val282	3.1
Asp298 N···O Met280	3.1
Leu303 N···O Asp298	3.1
Asp316 N···O Glu312	3.0
Ile379 N···O TPQ382	2.7
Asn381 N···O Ile379	3.3
TPQ382 N···O Ile379	3.2
Thr403 N···O Asp383	2.9
Val405 N···O Asn381	2.8
His431 N···O His592	3.2
His433 N···O *Leu590*	2.9
Leu590 N···O His433	2.9
His592 N···O His431	2.8

[a] The esds of the listed distances are 0.3−0.5 Å. [b] Residues which are neither conserved nor conservatively substituted in AGAO, ECAO, and PSAO are in italics. The following residues are conservatively substituted (Asp/Glu, Lys/Arg, Ser/Thr, and Ile/Val): Lys354, Asp357, Ile379, Thr403, Val405, and Asp598. All other residues in the table are conserved in the three AOs. [c] Residues belonging to the same subunit as the Cu atom and TPQ cofactor are identified by their residue numbers. Residues belonging to the other subunit are identified by a prime (′). The alternative orientation of the TPQ phenolic ring is indicated by (alt). [d] Short contact. See also footnote a. [e] This contact lies outside the normally accepted range of bond angles at the donor and/or acceptor atom.

position is not suitable for the formation of an intersubunit disulfide bridge. In the case of Cys636, the entire residue is in a C-terminal part of the polypeptide for which there is no electron density. The possibility of an inter-subunit disulfide bridge at Cys636 cannot be excluded, but the evident disorder of the polypeptide argues against it. The same logic was previously applied to the corresponding residue in PSAO, Cys647 (*10*).

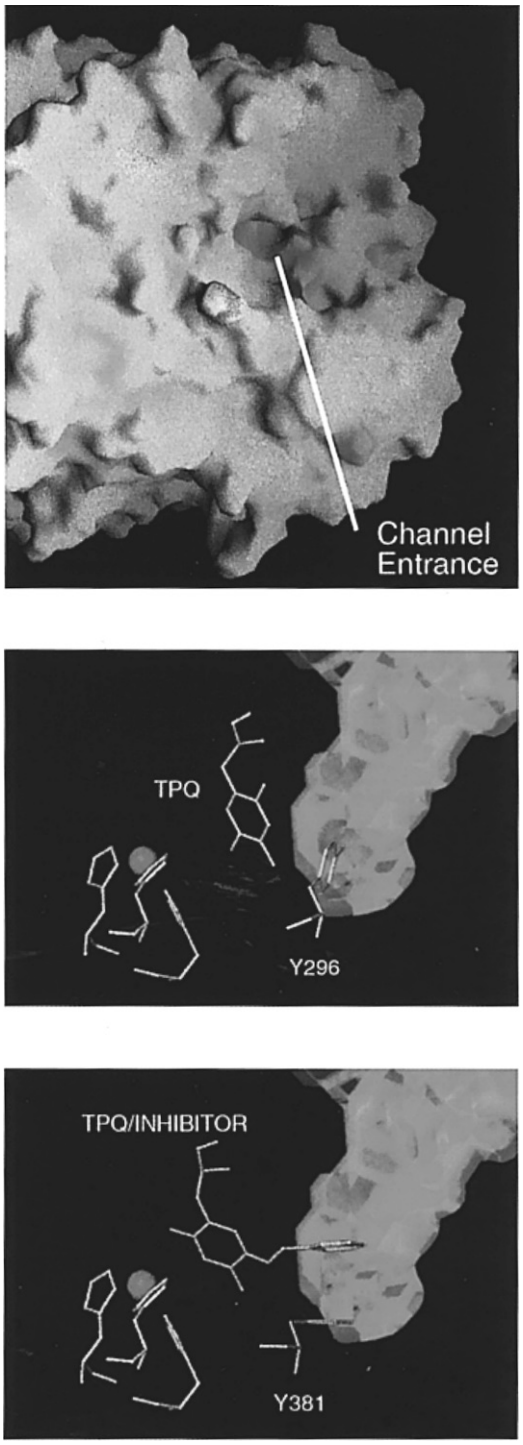

FIGURE 5: Channel from the molecular surface to the active site. (a, top) The surface of the holo-AGAO molecule, as seen by an observer looking upwards from the bottom of Figure 1b. Only the right-hand half of the molecule is shown. Colors indicate electrostatic charge density (red, negative; blue, positive). The entrance to the channel, surrounded by predominantly negative charges, is marked. The surface and charges were calculated using GRASP (*28*). (b, middle) The channel in relation to the active site of holo-AGAO. At the end of the channel, the Tyr296 gate is shown in the closed position. (c, bottom) A composite diagram incorporating the channel and Cu site of holo-AGAO from panel b and the TPQ−2-hydrazinopyridine inhibitor complex of ECAO (*9*). The Tyr381 gate in the inhibitor complex is shown in the open position. The programs used to calculate the molecular boundary and the channel were the same as those used for Figure 1d.

Second Metal Site. There is evidence that AGAO, like PSAO and ECAO, has a second metal site. However, one

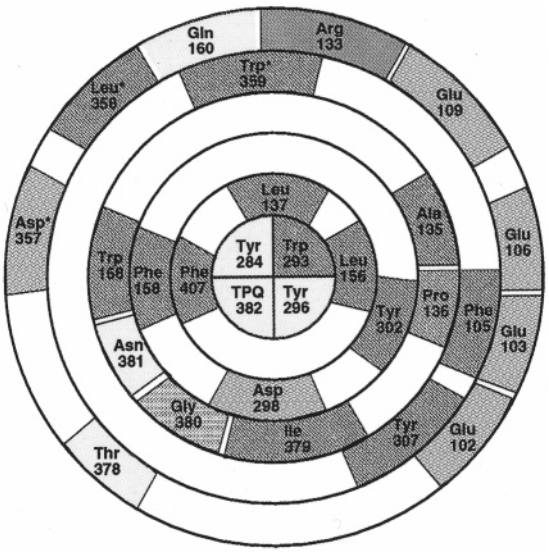

FIGURE 6: Schematic diagram of the interior of the channel from the molecular surface to the active site in AGAO, showing that the channel becomes increasingly hydrophobic as it approaches the active site. The circles represent sections through the channel, the radius decreasing as the distance from the surface increases. Residues lining the channel are color-coded: blue, hydrophobic; red, acidic; green, basic; yellow, polar uncharged; and gray, glycine. Residues Asp357, Leu358, and Trp359 are located on arm I of the other subunit and are marked by asterisks (*).

of the six groups which coordinate the second metal in PSAO and ECAO is missing; the residue corresponding to Asp453 in PSAO is Ala441 in AGAO. The remaining donor atoms lie at five of the six corners of an approximate octahedron. The electron density at the putative second metal site is consistent with either partial occupancy by a first-row transition metal atom or complete occupancy by a lighter metal atom such as Mg or Na and has been modeled as Mg. The distances of the potential coordinating atoms from the metal atom are as follows: $O^{\delta 1}$ Asp440, 2.7 Å; O Met441, 2.5 Å; $O^{\delta 2}$ Asp581, 2.7 Å; O Ile582, 2.7 Å; and O (water), 3.1 Å. The cited distances refer to the active form of the holoenzyme; the values in the other two forms of AGAO are not significantly different.

Comparisons between AGAO, ECAO, and PSAO: The Polypeptide Fold. The polypeptide fold of AGAO (prokaryotic) is closely similar to the folds previously reported for ECAO (prokaryotic) and PSAO (eukaryotic). A feature of technical interest is the fact that AGAO is the first AO where the relationship between the two subunits is rigorously defined in the crystal by a crystallographic 2-fold axis, in contrast with ECAO and PSAO, where the two subunits are related by noncrystallographic symmetry. When the three polypeptides are superimposed, large regions of structural homology are revealed (Figure 7). The structurally homologous regions include most of the invariant and conservatively substituted residues (Figure 7). The most notable difference among the three structures is that AGAO and PSAO lack the N-terminal domain D1 found in ECAO; AGAO, like PSAO, is "a mushroom without the stalk".

In pairwise superpositions of AGAO (active holo form) with PSAO and ECAO, the rms differences between corresponding C^{α} atom positions are 1.5 and 1.5 Å (whole molecule), 1.5 and 1.3 Å (one subunit), 1.4 and 1.6 Å (domain D2), 1.3 and 1.1 Å (domain D3), and 1.2 and 1.2 Å (domain D4), respectively. There are small systematic differences between the relative orientations of the three domains. When AGAO is compared with PSAO, the orientations of domains D2 and D3 in relation to domain D4 differ by rotations of 2.5 and 9.6°, respectively; when AGAO is compared with ECAO, the corresponding rotations are 4.4 and 5.3°.

Comparisons between AGAO, ECAO, and PSAO: The Cu/TPQ Site. In Figure 2, we compare the active sites of holo-AGAO (active and inactive), PSAO (active), and ECAO (inactive). In all four structures, the Cu(II) atom is coordinated by the N^{ϵ}(imidazole) atoms of two histidine residues and the N^{δ}(imidazole) atom of the third histidine. In the active forms of AGAO and PSAO, the Cu(II) atom has, in addition, two coordinated water molecules, resulting in an approximately square-pyramidal Cu(II) site geometry (Figure 2a,e). In the inactive forms of AGAO and ECAO, the Cu(II) atom is four-coordinate and trigonal-pyramidal to tetrahedral (Figure 2b,f). These similarities are consistent with evidence from comparative spectroscopic studies showing that the structure of the Cu(II) site is highly conserved among amine oxidases (see, e.g., ref 3).

The finding that one of the Cu-binding residues in AGAO, His592, exists as two conformers was not predicted spectroscopically, and is tentatively assigned to a loss of Cu (see Disorder at a Cu-binding Histidine). No disorder has been reported for the corresponding residues His603 in PSAO and His689 in ECAO. However, there appears to be disorder at one of the other Cu-binding histidines in the structure of the ECAO−inhibitor complex (*9*). The disordered residue in ECAO is His524, which corresponds to His431 in AGAO. The possibility of Cu sites in which this histidine is not coordinated to the Cu atom has been mentioned (*9*).

In the active form of holo-AGAO, the TPQ side chain occupies, within the limits of precision, the same position as in PSAO (active), while in the inactive form, its position is the same as in ECAO (inactive). As already stated, the orientation of the quinonoid ring is not defined adequately by the electron-density maps for either form of holo-AGAO. In contrast, the earlier structure analysis of PSAO left no doubt that the TPQ in the resting state of that molecule has C═O5 oriented toward the Cu atom (see Figure 7 in ref 10). In view of the strong and increasing evidence showing that the TPQ side chain in amine oxidases is highly flexible (*10*), the orientation of the aromatic group may be less important in a mechanistic sense than its position in relation the rest of the active site.

Since there are no precedents for the structure of apo-AGAO, the only comparisons that can be made with ECAO or PSAO refer to the holoenzymes. The structure analysis of apo-AGAO has confirmed the absence of a Cu atom, has shown that the active-site histidine side chains have positions similar to those in the holoenzyme, and has clearly defined the position of the unmodified Tyr382 side chain. The position of the tyrosine phenol ring is similar to that of the TPQ quinone ring in the inactive forms of holo-AGAO and ECAO, and is therefore significantly different from that of the TPQ quinone ring in the active form of holo-AGAO and in PSAO. The two sets of locations are related by rotations of ~120° about $C^{\alpha}-C^{\beta}$ and ~60° about $C^{\beta}-C^{\gamma}$, respectively (Table 3b). The phenolic OH in apo-AGAO in fact lies close to the position of the corresponding TPQ atom, O4, in the inactive forms of AGAO and ECAO. If a Cu atom were

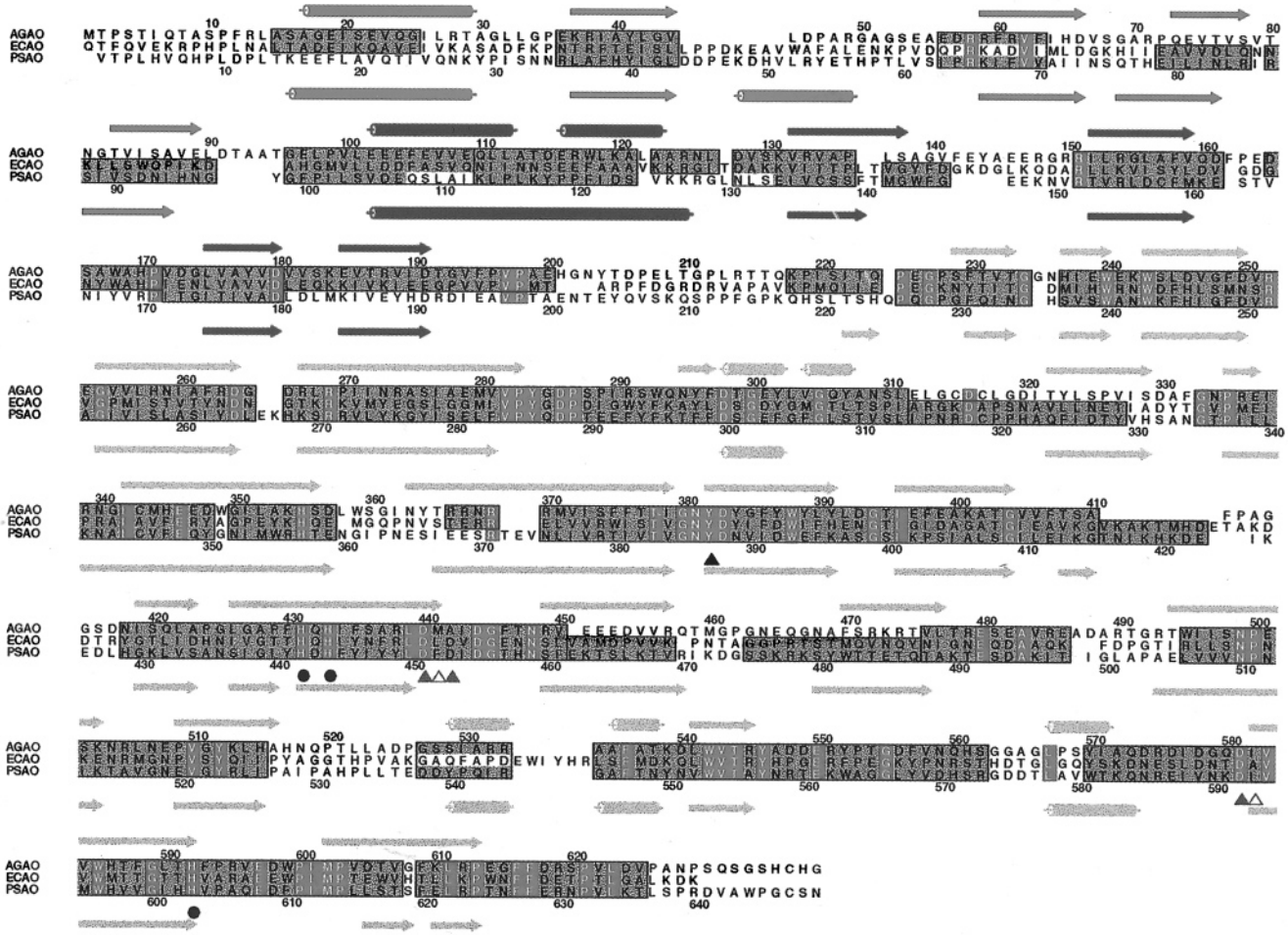

FIGURE 7: Structure-based alignment of the amino acid sequences of AGAO, ECAO, and PSAO. The residue numbers for AGAO and PSAO are shown above the first line and below the third line. Part of the N-terminal sequence of ECAO, which is not coded in AGAO and PSAO, is omitted. Elements of secondary structure in AGAO and PSAO are indicated as arrows (β-strands) and cylinders (helices), with color coding to indicate subunit domain 2 (red), domain 3 (green) and domain 4 (yellow). Structurally conserved regions, defined as they were previously (*10*), are shaded gray. The assignments of secondary structure were made using DSSP (*44*), and the structurally conserved regions were identified using ALSCRIPT (*45*). Sequence identity among the three proteins is indicated by red residue symbols. The three Cu-binding His residues are marked with blue circles. The residues where a second metal is bound in ECAO and PSAO are marked as brown triangles [filled where the metal is coordinated at an Asp side chain and empty where the metal is coordinated at the O (peptide) atom]. A black triangle denotes the TPQ.

present, the phenolic OH would be in a position suitable for Cu−O bonding.

Channels to the Active Site in AGAO, ECAO, and PSAO. The channel from the molecular surface to the active site is described for the first time in AGAO (Figure 5). The key to the recognition of the channel in AGAO was the absence of electron density corresponding to the phenol ring of Tyr296, leading to the omission of this side chain from the model; an observer outside the molecule then had an unobstructed view of TPQ at the active site. We find that a similar channel exists in PSAO and ECAO, though the channel in PSAO crystals is narrower than in AGAO, and the channel in ECAO crystals is partly obstructed. The reasons why these channels were missed in earlier descriptions are of interest. In PSAO, the bottom of the channel is blocked by Phe298. In the structure analysis, the electron density of Phe298 was well-defined, and the side chain was modeled in a single conformation which obscured the active site when the structure was viewed from the direction of the channel. We assume that, although Phe298 is ordered in the crystal structure of PSAO, it has the same flexibility that is suggested in AGAO by the disorder of the corresponding residue, Tyr296. In ECAO, the channel can be identified once one knows where to look for it. However, in this structure, the channel is partly obstructed, and the accessibility of the active site depends on the movement of several side chains. The active site is again hidden from view, this time by the side chain of Tyr381. In the recently reported structure of an ECAO−inhibitor complex (*9*), Tyr381 is rotated out of the way, and the TPQ-bound hydrazinopyridine inhibitor extends from the active site into a region which corresponds to the channel in AGAO (Figure 5c). Thus, there is ample evidence showing that the channel provides the required access of the substrate to the active site. Further, the active site has a gate, and this is seen in the closed (PSAO), open (ECAO), and swinging (AGAO) states.

β-Ribbon Arms in AGAO, ECAO, and PSAO. When AGAO, ECAO, and PSAO are superimposed, the central, antiparallel β-ribbon portions of arm I occupy closely similar positions (Figure 8). The main difference between these segments is that they contain different numbers of residues (AGAO, 22; PSAO, 25; and ECAO, 21) so that they extend to different positions on the molecular surface. In all three proteins, the end of arm I makes contact with domain D3 near the entrance to the channel from the surface to the active site, and the residues at the end of arm I form part of the

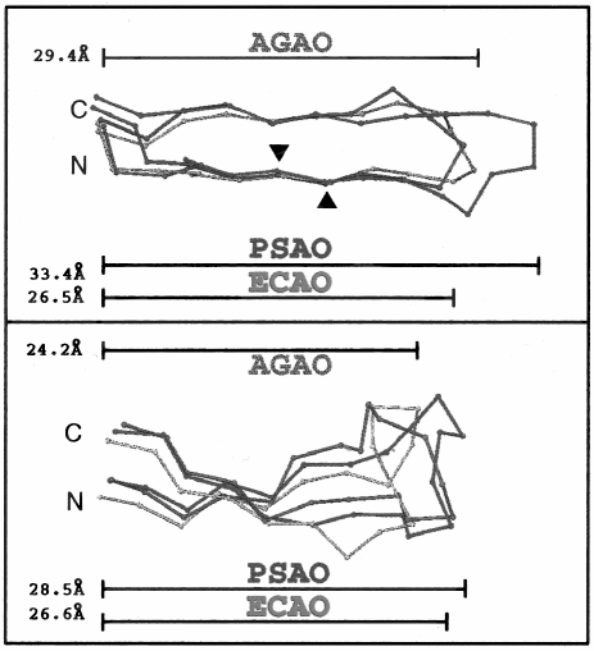

FIGURE 8: Semiquantitative comparison between the intersubunit arms in PEAO, PSAO, and ECAO, drawn as C^{α} diagrams. The orientation is approximately the same as that in Figure 1c (upper, arm I; lower, arm II). The alignment was obtained by superimposing the three entire molecules. The central portions of arm I are almost exactly aligned so that the residues corresponding to Lys354 (▼) and His355 (▲) in AGAO occupy the same position in all three proteins. The conformations of arm II are more varied. The lengths of the two arms (in angstroms) are measured from corresponding residues at the left-hand edge of the Figure.

entrance to the channel. In AGAO, these residues are Asp357, Leu358, and Trp359 (Figure 6); in PSAO, Thr358, Glu359, Asn360, and Gly361; and in ECAO, Gln441, Glu442, and Met443. The different shapes and bulks of these residues are noteworthy.

The superimposable portions of arm I pass close to the active site, and include two residues which appear to be invariant or conservatively substituted (Figure 7). These are an invariant histidine (His355 in AGAO, His440 in ECAO, and His357 in PSAO) and the conservatively substituted neighboring residue (Lys354 in AGAO, Lys439 in ECAO, and Arg356 in PSAO). The hydrogen bonds and salt bridges involving His355 and Lys354 in AGAO have been described above (see Active Sites in Holo-AGAO and Figure 4). Analogous interactions in PSAO have been noted (*10*). The significance of these interactions may be that they stabilize the position of the polypeptide backbone in the vicinity of the active site in relation to arm I, or vice versa.

In contrast with arm I, the conformational differences between the segments labeled arm II in AGAO, ECAO and PSAO are relatively large (Figure 8). Further, there are no conserved interactions between arm II and residues at, or near, the active site. In PSAO, the N (indole) atom of Trp482 on arm II is hydrogen bonded to the carboxylate group of active-site residue Asp443 (*10*). Neither residue is conserved in other amine oxidases, the corresponding residues in AGAO being Phe470 and Gln432. Phe470 does make a contact consistent with hydrogen bonding, but this involves only its backbone amide group and the side chain of Asn418. In addition, the side chain of Asn468 on arm II interacts with the backbone amide group of Tyr284 in domain D4. Among the four residues involved in these two hydrogen bonds in AGAO, only Tyr284 is conserved. The interactions do not seem to be sufficiently specific to contribute to the active-site properties. For the time being, the most likely reason for the existence of arm II is that it contributes to the structural stability of the dimer.

Solvent-Filled Cavity in AGAO, ECAO, and PSAO. The unusual solvent-filled cavity between the two D4 domains of AGAO also occurs in ECAO and PSAO. The volumes of the cavity in the three proteins as traced by a 1.4 Å rolling sphere are ~3950 $Å^3$ (corresponding to ~130 solvent molecules), ~2430 $Å^3$ (~80 solvent molecules), and ~8250 $Å^3$ (~270 solvent molecules), respectively. As stated earlier in the description of AGAO, the wall of the cavity includes a segment of β-sheet which has two of the Cu-binding active-site histidine side chains on its other side. Only the backbone atoms of these histidine residues are in contact with the solvent in the cavity. Within the active site, the two histidine residues are on the side remote from the TPQ cofactor so that substrate amines and product aldehydes are unlikely to enter or leave the active site from this direction. However, there remains a possibility that the cavity is a route for the diffusion of Cu^{2+} ions, O_2 molecules, H_2O_2 molecules, and/or NH_4^+ ions between the molecular surface and the active site.

Comments on the "Plug" or "Lid" in AGAO, ECAO, and PSAO. In the original descriptions of ECAO and PSAO, attention was drawn to a plug or lid comprising a short three-stranded β-sheet and a short segment of helix. The possibility that a movement of the plug or lid permits access to the active site was discussed (*8*, *10*). A feature with a similar β-sheet structure is present in AGAO at residues 408−428, but the short helix is reduced to a loop. The hypothesis that access to the active site depends on a movement of the plug is less persuasive in light of the evidence from this work showing that there is a channel from the solvent to the active site.

STRUCTURAL SPECULATIONS

Structures of the Cu Amine Oxidase Active Site. This work and antecedent structural studies provide four snapshots of the Cu amine oxidase active site. (i) The apo-AGAO structure shows the three active-site histidine residues and the reactive Tyr ready to coordinate the Cu(II) ion. (ii) In the inactive (TPQ-ON) form of holo-AGAO and ECAO, the coordination of the Cu(II) atom by the three histidines and the TPQ has occurred. The coordination geometry is not well-defined. If the bond angles at the Cu atom in inactive holo-AGAO were taken literally, the geometry would be described as trigonal-pyramidal with two histidines and the TPQ at the base and the third histidine at the apex. The coordination geometry in ECAO was described in closely similar terms (*8*). Neither structure is determined precisely enough to exclude the possibility that the geometry is actually tetrahedral, or that the Cu atom has an additional water ligand. In both structures, there is ample room for the Cu atom to accommodate an additional ligand such as H_2O or O_2. (iii) In the active (TPQ-OFF) form of holo-AGAO and PSAO, the Cu atom has a square-pyramidal geometry, with the three histidines and a water molecule as the equatorial ligands and a second water molecule as the axial ligand. The locations of the two water molecules are not determined precisely by the crystallographic analyses, but can be inferred

Scheme 1: Biogenesis of TPQ

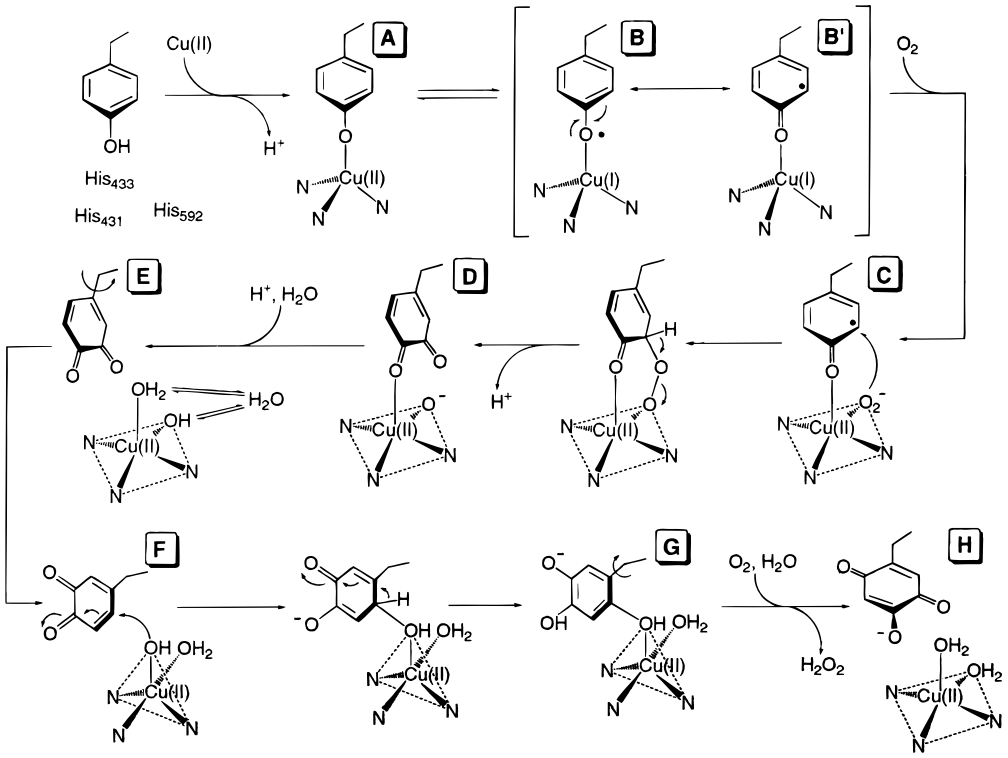

unequivocally from spectroscopic data (*3*). The TPQ cofactor is close, but not coordinated, to the Cu atom. In AGAO crystallized at pH ~8, the orientation of the TPQ quinone ring is not defined by the electron density at the present resolution. In PSAO crystallized at pH ~5, the orientation of the TPQ quinone ring is such that a rotation of ~180° about the $C^{\beta}-C^{\gamma}$ bond must occur when the substrate reacts at C=O5 (*10*). (iv) Finally, in the structure of an ECAO−inhibitor complex (*9*), the TPQ quinone ring is seen in the predicted orientation, i.e., flipped by ~180° from the orientation in PSAO.

Biogenesis of the TPQ Cofactor. In Scheme 1, we use the first three of the above snapshots as steps in a mechanism for the biogenesis of the TPQ cofactor. In a previous version of this mechanism (*14*), the Cu atom was treated as an appendage of the polypeptide without any specific consideration of geometrical requirements. Scheme 1 incorporates what we now know about the geometry of the Cu site.

In the first step of Scheme 1, a Cu^{2+} ion binds to the apoprotein to form a Cu(II) complex, **A**. The complex **A** is in equilibrium with a Cu(I)−tyrosyl radical, **B**. The unpaired spin in **B** is delocalized over the aromatic ring, activating the ring carbon atoms, as drawn in the resonance form **B′**. The Cu(I) complex reacts with dioxygen to form an activated oxygen complex, shown here as a Cu(II)−superoxide, **C** (*30*). This activated oxygen complex attacks the tyrosyl radical, forming a dopaquinone bound to a Cu(II) oxide/hydroxide/aqua complex, **D**. The Cu(II) oxide/hydroxide/aqua species should be in rapid exchange with solvent water, ultimately permitting solvent oxygen incorporation into TPQ, **E** → **F**. We suggest that small movements of the Cu atom and the coordinating groups now result in a change from square-pyramidal to trigonal-bipyramidal coordination.[3] The main effect of this change is that the previously axial water/hydroxo ligand becomes equatorial, which should increase its acidic character. Rotation of the dopaquinone aromatic ring brings C2 close to the now-equatorial water/hydroxo ligand, **F**. Nucleophilic attack by the Cu(II)−OH^- on the dopaquinone (which should be highly susceptible to nucleophilic attack) yields topa, **G**. In the presence of dioxygen, topa is then rapidly oxidized to TPQ. Following dissociation of the TPQ, the Cu(II) atom picks up a water molecule and returns to a square-pyramidal geometry, **H**.

All the steps in Scheme 1 are geometrically feasible. The structure of the apoprotein is known. The essential features of **A** and **B** are present in the TPQ-ON forms of AGAO and ECAO. The current structures of these two TPQ-ON forms are also consistent with the proposed change from quasi-tetrahedral to square-pyramidal coordination by the addition of a dioxygen ligand at **C**. Steps **C** → **D** → **E** → **F** → **G** have been checked by computer-graphics simulations, in which the structures of TPQ-ON and TPQ-OFF holo-AGAO were used as starting models. The Tyr/TPQ side chain was permitted only to rotate about the $C^{\alpha}-C^{\beta}$ and $C^{\beta}-C^{\gamma}$ bonds, and the geometry of the Cu atom was permitted to vary only among the quasi-tetrahedral, square-pyramidal, and trigonal-bipyramidal configurations described in the text. At steps **C** → **D** and **F** → **G**, it was confirmed that the conformational changes required to permit a C···O distance of 3.5 Å are plausible. (This distance is assumed to be the upper limit for chemical interaction.) At the end of the reaction sequence, **H**, the active site is in a resting state as found in the TPQ-OFF forms of holo-AGAO, ECAO, and PSAO.

The chemistry required for the various steps of Scheme 1 is known. Direct conversion of phenols to *o*-quinones (**A**

[3] The change from square-pyramidal geometry [His431, His433, His592, $O_{w(eq)}$ equatorial, and $O_{w(ax)}$ axial] to trigonal-bipyramidal geometry requires only a small movement of the Cu in the direction of $O_{w(ax)}$, small movements of His433 and His592 in the opposite direction, and a slight lengthening of the bonds from the Cu to His431 and $O_{w(eq)}$. The new equatorial ligands are His433, His592, and the former $O_{w(ax)}$; the new axial ligands are His431 and the former $O_{w(eq)}$.

Scheme 2: Catalytic Cycle[a]

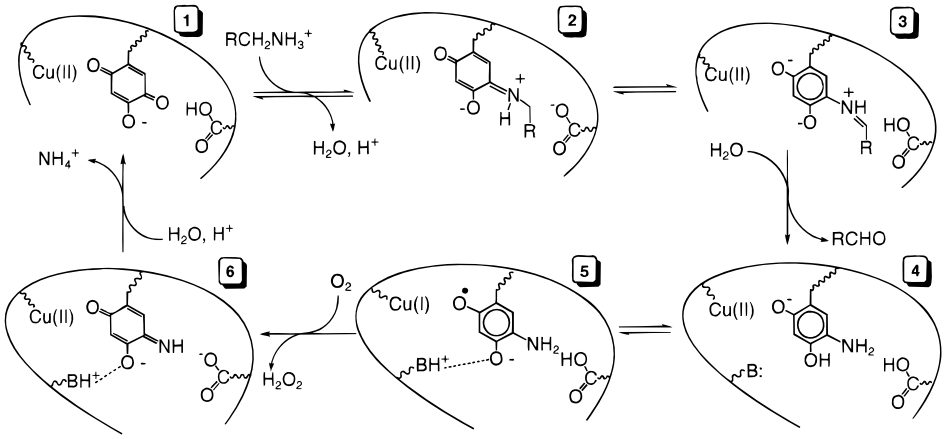

[a] Adapted from ref 10.

→ **D**) by Cu(I) in the presence of O_2 has been demonstrated, and an intermediate similar to that shown between **C** and **D** has been suggested (*31*). There are good precedents for copper-mediated phenol oxidation (*32*), the reactivity of Cu(I) complexes with N-donor ligands toward O_2 (*33*), and the nucleophilicity of metal-coordinated hydroxides (*34*). The conversion of 4-methylcatechol (possibly in the anion form) to 2-hydroxy-5-methyl-1,4-benzoquinone in the presence of Cu(II) and O_2 under quasi-physiological conditions provides a model reaction for the conversion of dopa- to topaquinone (*35*). Phenoxyl radical intermediates are implicated in the copper-mediated oxidation of phenols (*36*). The solvent origin of the C2 carbonyl oxygen at **F** has been established by isotope labeling and resonance Raman spectroscopy (*37*), though it has been suggested that slight doubts connected with the pretreatment of the protein need to be resolved (*14*). There are two reasonable mechanisms for the final step (**G** → **H**). Reduced quinones may be oxidized by O_2 even in the absence of metals. Alternatively, the reaction may be facilitated by intracomplex electron transfer to Cu(II) to produce a Cu(I)−semiquinone, which then reacts with O_2 (*38*). The production of H_2O_2 during TPQ formation has been detected (D. M. Dooley and C. E. Ruggiero, unpublished results).

While much of Scheme 1 is still in the realm of structural speculation, it complements some of the results of recent kinetics and spectroscopic studies of TPQ formation (*14*). We have used the structures of apo-AGAO and TPQ-ON holo-AGAO to suggest a model **A** for the precursor protein−Cu(II) complex which is formed when Cu(II) is added to the apoprotein under anaerobic conditions. The change from axial tyrosine coordination in the precursor complex **A** to axial solvent coordination in the mature, resting enzyme **H** should be reflected in substantial spectroscopic differences. Consistent with this expectation, the Cu(II) ligand-field bands and EPR features of the precursor complex differ significantly from those of the resting enzyme (*14*). The qualitative description in which the EPR signal of the precursor complex "typical of tetragonal Cu(II) complexes" implies that the proposed model **A** has a $d_{x^2-y^2}$ ground state. Since the geometry of model **A** is by no means rigidly defined, it may well be able to satisfy this criterion.

Once dioxygen is admitted, the precursor protein−Cu(II) complex mentioned above becomes competent for the oxidation of tyrosine to TPQ (*14*). Axial ligation may contribute to the reaction in two ways; it may activate the Cu(II)−O−Ph moiety **A** for direct oxidation [analogous with a proposed mechanism for intradiol-cleaving catechol dioxygenases (*39*)], or it may provide a favorable geometry for electron transfer from Tyr382 to form the Cu(I)−O−$Ph^{\bullet+}$ moiety, **B**. In the latter case, axial ligation may also influence the delicate balance required for the reaction via a phenoxyl radical intermediate; the formation of the tyrosine radical must be promoted, but the radical must not be stabilized sufficiently to hinder its further oxidation. Consequently, the equilibrium **A** ⇌ **B** in Scheme 1 would be expected to lie to the left, but **B** must be sufficiently reactive to undergo reaction with the Cu(II)−O_2^- intermediate at **C**. Provided that the tyrosine radical remains in the Tyr382 position seen in the apo-AGAO structure, it should be well-positioned for oxygen-atom transfer from the Cu(II)−O_2^- intermediate to C3 at step **C**. In contrast with the implied activation of the axial tyrosine at step **C**, the equatorial coordination of a tyrosine radical to Cu(II) in the Cu−enzyme galactose oxidase is known to provide substantial stabilization. The equatorially coordinated tyrosine radical in that protein appears to be resistant to oxidative reactions (*40*).

Catalytic Mechanism. Although the structures of inactive (TPQ-ON) and active (TPQ-OFF) holo-AGAO provide few surprises, they help to confirm the key elements of the currently accepted catalytic cycle (Scheme 2). The fact that the relative positions of the Cu site, the TPQ side chain, and the active-site aspartic acid residue are conserved in AGAO, PSAO, and ECAO (Figure 2) firmly establishes these groups as the catalytic "triad" of copper-containing amine oxidases. The redox role attributed to the Cu in step **4** → **6** of Scheme 2 is consistent with all our current information on the active-site structure, and is supported by the conserved proximity of the Cu atom to the TPQ. The formal analogy between the reoxidation of the substrate-reduced enzyme in catalytic turnover (**5** → **6** in Scheme 2) and the oxidation of the reduced quinone in TPQ biogenesis (**G** → **H** in Scheme 1) is one of the factors which led to our suggestion that the Cu atom participates in the latter reaction.

The difference between the TPQ side chain conformations in the inactive and active forms of holo-AGAO confirms similar observations for ECAO (*8*, *9*). The subtle nature of this difference is emphasized by the fact that the two forms of holo-AGAO were grown under almost identical conditions. It appears that the reported connection between

exposure to $(NH_4)_2SO_4$ and inactivation of the enzyme (*8*) requires re-assessment.

It is unfortunate that several interesting questions concerning the holo-AGAO structure cannot be answered until X-ray data of higher quality and resolution become available. Does our difficulty in defining the orientation of the TPQ quinone ring merely reflect the quality of the current X-ray data, or is the orientational disorder of the TPQ quinone ring in AGAO really greater than that in PSAO? Does the apparent lack of a hydrogen bond between the TPQ and the active-site base Asp298 merely reflect the large esds of the atomic positions, or does it represent another real difference between AGAO and PSAO? Since AGAO was crystallized at pH ~8.1 whereas PSAO was crystallized at pH ~4.8, real differences between the active-site structures would clearly have important mechanistic implications.

Scheme 2 does not attempt to model the considerable variability in the turnover rates and stereochemistries of amine oxidases. The relevant aspects of amine oxidase reactivity may include enzyme−substrate recognition, access of substrate molecules to the active site, and interactions between the TPQ or reaction intermediates with additional active-site residues or active-site water molecules. Some of these aspects are addressed in the following sections.

Mechanistic Implications of the Channel with Respect to the Active Site. The identification of a gated channel from the molecular surface to the active site has, in principle, answered an important question which was not resolved satisfactorily by previous structure analyses: how do substrates reach the active site? We now suggest that the channel does not merely provide a pathway for substrates, but plays a role in facilitating the catalytic reaction. Two items from the description of the channel in AGAO are relevant (see A Channel to the Active Site). The entrance to the channel is surrounded by predominantly negative surface charges, and the channel becomes increasingly hydrophobic as it approaches the active site (Figure 6). Similar descriptions apply to PSAO and ECAO. This gradation of properties appears to be ideal for an enzyme which has to recognize RNH_3^+, but which processes RNH_2. The predominantly negative surface charges should provide electrostatic guidance for small, positively charged molecules such as amine substrates, as well as for aquated Cu^{2+} ions. The gradation of charge effects along the channel should favor deprotonation of the substrate amine group in the upper, more basic regions, leaving a neutral primary amine group as required for addition to the reactive C═O5 carbonyl of TPQ.

Once a substrate molecule has reached the bottom of the channel, there are two ways in which the dynamics of localized protein conformational changes may contribute to the catalytic reaction: gating by Tyr/Phe at the base of the channel and reorientation of the TPQ side chain. Whenever the TPQ side chain is in the orientation seen in the resting structures of PSAO and (possibly) AGAO (Figure 2e,a), it must undergo a rotation so that its C═O5 carbonyl group is correctly positioned for reaction with the substrate primary amine group. The possibility of "concerted action in which the nucleophilic amine substrate attacks at C5 .... and the TPQ aromatic group rotates" has been indicated previously (*10*).

Structural Aspects of Substrate Preference. It has long been recognized that, while copper-containing amine oxidases generally oxidize a variety of primary amines, the relative rates vary significantly from enzyme to enzyme. For example, AGAO oxidizes a range of aromatic alkyl primary amines. The enzyme is induced by growth on phenylethylamine, so phenylethylamine is considered the preferred substrate. In the case of PSAO, the preferred substrates are primary diamines. ECAO has a broader substrate specificity, oxidizing both aromatic and alkyl primary amines. These distinctive patterns of substrate preference appear to be in conflict with the close similarity between the active site structures of the enzymes (Figure 2). If the active sites are so similar, why are the catalytic activities in some cases so different?

This work leads to the hypothesis that substrate recognition is yet another function mediated by the channel from the protein surface to the active site. The mediation may occur either via structural motifs that differentiate among amines or via facilitated transport of preferred substrates. At least three features may be relevant. (i) The partial obstruction of the channel in ECAO, in contrast with the uncluttered channels in AGAO and PSAO, suggests that the channel in each protein has a distinct internal architecture. (ii) Additional steric and electrostatic differences occur at the entrances to the channels. While the side chains near the entrance to the channel in AGAO, PSAO, and ECAO are predominantly negative, they are different in each protein. (iii) The β-ribbon arm I which reaches along the surface of the molecule to the channel entrance may play a role in creating these features, since the residues at the end of arm I in each protein are different in bulk, shape, and charge distribution (see β-Ribbon Arms above).

The combination of features i−iii bestows on each protein a distinctive distribution of surface charges and a distinctive molecular surface topology. Since amine substrates are recognized in their protonated, positively charged form, the electrostatic potential and surface topology at the entrance to the channel may be important for substrate recognition. The sequence of side chains along the interior surface of the channel, flexible though they presumably are, may also affect substrate recognition by fine-tuning the tendency of the substrate to lose a proton prior to interacting with the active-site TPQ.

CONCLUSIONS

This work leads to five significant advances in the description of amine oxidase structures. (i) AGAO is the first amine oxidase where structural comparisons between the active sites in the precursor apoprotein and two forms of the holoprotein are possible. The structures of the active and inactive forms of holo-AGAO confirm many of the details in the earlier descriptions of PSAO (active) and ECAO (inactive). (ii) The problem of access to the active site from the molecular surface appears to have been solved by the discovery of a channel in AGAO, beginning near the junction of domains D3 and D4. Inspection of molecular models based on the deposited coordinates shows that a similar channel is present in PSAO and, in a less continuous form, in ECAO. It is suggested that the channel not only permits the transport of substrates and reaction products to and from the active site but also influences two other aspects of enzyme activity: the conversion of cationic amine substrates to the neutral form required for reaction with the TPQ

cofactor and the molecular recognition of different types of substrate. (iii) In view of point ii, the hypothesis that access to the active site requires the movement of a plug or lid on the molecular surface (*8*, *10*) is probably unnecessary. (iv) The large interface between the two D4 domains of the dimeric molecule is not continuous, but is an annulus surrounding a large solvent-filled cavity. We have described this cavity in some detail for AGAO, and have confirmed the presence of similar cavities in ECAO and PSAO by inspecting models. (v) The fact that AGAO has arms closely similar to those found in ECAO and PSAO supports the hypothesis that the arms are essential features of the molecule, with potential functions in the stabilization of the active site and in substrate recognition.

ACKNOWLEDGMENT

We thank Professor N. Sakabe for access to the Weissenberg diffraction camera on beamline 6A2 at the KEK Photon Factory.

REFERENCES

1. McIntire, W. S., and Hartmann, C. (1993) in *Principles and Applications of Quinoproteins* (Davidson, V. L., Ed.) pp 97−171, Marcel Dekker, New York.
2. Klinman, J. P., and Mu, D. (1994) *Annu. Rev. Biochem. 63*, 299−344.
3. Knowles, P. F., and Dooley, D. M. (1994) in *Metal Ions in Biological Systems* (Sigel, H., and Sigel, A., Eds.) Vol. 30, pp 361−403, Marcel Dekker, New York.
4. Fontecave, M., and Eklund, H. (1995) *Structure 3*, 1127−1129.
5. Anthony, C. (1996) *Biochem. J. 320*, 697−711.
6. Klinman, J. P. (1996) *J. Biol. Chem. 271*, 27189−27192.
7. Mure, M., and Tanizawa, K. (1997) *Biosci., Biotechnol., Biochem. 61*, 410−417.
8. Parsons, M. R., Convery, M. A., Wilmot, C. M., Yadav, K. D. S., Blakeley, V., Corner, A. S., Phillips, S. E. V., McPherson, M. J., and Knowles, P. F. (1995) *Structure 3*, 1171−1184.
9. Wilmot, C. M., Murray, J. M., Alton, G., Parsons, M. R., Convery, M. A., Blakeley, V., Corner, A. S., Palcic, M. M., Knowles, P. F., McPherson, M. J., and Phillips, S. E. V. (1997) *Biochemistry 36*, 1608−1620.
10. Kumar, V., Dooley, D. M., Freeman, H. C., Guss, J. M., Harvey, I., McGuirl, M. A., Wilce, M. C. J., and Zubak, V. M. (1996) *Structure 4*, 943−955.
11. Li, R., Chen, L., Cai, D., Klinman, J. P., and Mathews, F. S. (1997) *Acta Crystallogr. D 53*, 364−370.
12. Matsuzaki, R., Fukui, T., Sato, H., Ozaki, Y., and Tanizawa, K. (1994) *FEBS Lett. 351*, 360−364.
13. Matsuzaki, R., Suzuki, S., Yamaguchi, K., Fukui, T., and Tanizawa, K. (1995) *Biochemistry 34*, 4525−4530.
14. Ruggiero, C. E., Smith, J. A., Tanizawa, K., and Dooley, D. M. (1997) *Biochemistry 36*, 1953−1959.
15. Freeman, H. C., Guss, J. M., Kumar, V., McIntire, W. S., and Zubak, V. M. (1996) *Acta Crystallogr. D 52*, 197−198.
16. Tanizawa, K., Matsuzaki, R., Shimizu, E., Yorifuji, T., and Fukui, T. (1994) *Biochem. Biophys. Res. Commun. 199*, 1096−1102.
17. Shimizu, E., Ohta, K., Takayama, S., Kitagaki, Y., Tanizawa, K., and Yorifuji, T. (1997) *Biosci., Biotechnol., Biochem. 61*, 501−505.
18. Otwinowski, Z. (1993) in *Proceedings of the CCP4 Study Weekend: Data Collection and Processing* (Sawyer, L., Isaacs, N. W., and Bailey, S. S., Eds.) pp 56−62, SERC Daresbury Laboratory, Warrington, U.K.
19. Collaborative Computational Project, No. 4 (1994) *Acta Crystallogr. D* 50, 760−763.
20. Sato, M., Yamamoto, M., Imada, K., Katsube, Y., Tanaka, N., and Higashi, T. (1992) *J. Appl. Crystallogr. 25*, 348−357.
21. Read, R. J. (1986) *Acta Crystallogr. A 42*, 140−149.
22. Navaza, J. (1994) *Acta Crystallogr. A 50*, 157−163.
23. Brünger, A. T. (1992) *X-PLOR, Version 3.1. A System for Crystallography and NMR*, Yale University Press, New Haven, CT.
24. Jones, T. A., Zou, J.-Y., Cowan, S. W., and Kjeldgaard, M. (1991) *Acta Crystallogr. A 47*, 110−119.
25. Kleywegt, G. J., and Jones, T. A. (1996) *Structure 4*, 1395−1400.
26. Laskowski, R. A. (1995) *J. Mol. Graphics 13*, 323−330.
27. Kleywegt, G. J., and Jones, T. A. (1994) *Acta Crystallogr. D 50*, 178−185.
28. Nicholls, A., Bharadwaj, R., and Honig, B. (1993) *Biophys. J. 64*, 166−170.
29. Farnum, M., Palcic, M., and Klinman, J. P. (1986) *Biochemistry 25*, 1898−1904.
30. Fujisawa, K., Tanaka, M., Moro-oka, Y., and Kitajima, N. (1994) *J. Am. Chem. Soc. 116*, 12079−12080.
31. Sayre, L. M., and Nadkarni, D. V. (1994) *J. Am. Chem. Soc. 116*, 3157−3158.
32. Spodine, E., and Manzur, J. (1992) *Coord. Chem. Rev. 119*, 171−198.
33. Karlin, K. D., Kacleci, S., and Zuberbühler, A. (1997) *Acc. Chem. Res. 30*, 139−147.
34. Wilcox, D. E. (1996) *Chem. Rev. 96*, 2435−2458.
35. Rinaldi, A. C., Porcu, M. C., Curreli, N., Rescigno, A., Finazzi-Agró, A., Pedersen, J. Z., Rinaldi, A., and Sanjust, E. (1995) *Biochem. Biophys. Res. Commun. 214*, 559−567.
36. Lyons, J. E., and Hsu, C.-Y. (1985) in *Biological and Inorganic Copper Chemistry* (Karlin, K. D., and Zubieta, J., Eds.) pp 57−76, Adenine Press, New York.
37. Nakamura, N., Matsuzaki, R., Choi, Y.-H., Tanizawa, K., and Sanders-Loehr, J. (1996) *J. Biol. Chem. 271*, 4718−4724.
38. Li, Y., and Trush, M. A. (1993) *Arch. Biochem. Biophys. 300*, 346−355.
39. Que, L., and Ho, R. Y. N. (1997) *Chem. Rev. 97*, 2607−2624.
40. Whittaker, J. W. (1994) in *Metal Ions in Biological Systems* (Sigel, H., and Sigel, A., Eds.) Vol. 30, pp 315−360, Marcel Dekker, New York.
41. Cruickshank, D. W. J. (1996) in *Macromolecular Refinement, Proceedings of the CCP4 Study Weekend January 1996* (Dodson, E., Moore, M., Ralph, A., and Bailey, S., Eds.) pp 11−22, SERC Daresbury Laboratory, Warrington, U.K.
42. Kraulis, P. J. (1991) *J. Appl. Crystallogr. 24*, 946−950.
43. Merrit, D. J., and Murphy, M. E. P. (1994) *Acta Crystallogr. D 50*, 869−873.
44. Kabsch, W., and Sander, C. (1983) *Biopolymers 22*, 2577−2637.
45. Barton, G. J. (1993) *Protein Eng. 6*, 37−40.

BI971797I